

## Transient HIF2A inhibition promotes satellite cell proliferation and muscle regeneration

Liwei Xie, ... , Jarrod A. Call, Hang Yin

*J Clin Invest.* 2018. <https://doi.org/10.1172/JCI96208>.

Research Article In-Press Preview Muscle biology Stem cells

The remarkable regeneration capability of skeletal muscle depends on coordinated proliferation and differentiation of satellite cells. The self-renewal of satellite cells is critical for long-term maintenance of muscle regeneration potential. Hypoxia profoundly affects the proliferation, differentiation, and self-renewal of cultured myoblasts. However, the physiological relevance of hypoxia and hypoxia signaling in satellite cells *in vivo* remains largely unknown. Here, we report that satellite cells are in an intrinsic hypoxic state *in vivo* and express hypoxia-inducible factor 2A (HIF2A). HIF2A promotes the stemness and long-term homeostatic maintenance of satellite cells by maintaining the quiescence, increasing the self-renewal and blocking the myogenic differentiation of satellite cells. HIF2A stabilization in satellite cells cultured under normoxia augmented their engraftment potential in regenerative muscle. Reversely, HIF2A ablation led to the depletion of satellite cells and the consequent regenerative failure in the long-term. In contrast, transient pharmacological inhibition of HIF2A accelerated muscle regeneration by increasing satellite cell proliferation and differentiation. Mechanistically, HIF2A induces the quiescence/self-renewal of satellite cells by binding the promoter of *Spry1* gene and activating *Spry1* expression. These findings suggest that HIF2A is a pivotal mediator of hypoxia signaling in satellite cells and may be therapeutically targeted to improve muscle regeneration.

Find the latest version:

<https://jci.me/96208/pdf>



# Transient HIF2A Inhibition Promotes Satellite Cell Proliferation and Muscle Regeneration

Liwei Xie,<sup>1,2,#</sup> Amelia Yin,<sup>1,2</sup> Anna S. Nichenko,<sup>3</sup> Aaron M. Beedle,<sup>4</sup> Jarrod A. Call,<sup>3,5</sup> Hang Yin<sup>1,2,\*</sup>

<sup>1</sup> Department of Biochemistry and Molecular Biology, University of Georgia, Athens, GA 30602, USA

<sup>2</sup> Center for Molecular Medicine, University of Georgia, Athens, GA 30602, USA

<sup>3</sup> Department of Kinesiology, University of Georgia, Athens, GA 30602, USA

<sup>4</sup> Department of Pharmaceutical Sciences, Binghamton University-SUNY, Binghamton NY 13902, USA

<sup>5</sup> Regenerative Bioscience Center, University of Georgia, Athens, GA 30602, USA

# Present address: State Key Laboratory of Applied Microbiology of Southern China, Guangdong Institute of Microbiology, Guangzhou, Guangdong, 510070, China

\* Corresponding author:

Center for Molecular Medicine, University of Georgia, Athens, GA 30602, USA

Phone: (706) 583-0655

Email: [hyin@uga.edu](mailto:hyin@uga.edu)

The authors have declared that no conflict of interest exists.

## ABSTRACT

The remarkable regeneration capability of skeletal muscle depends on coordinated proliferation and differentiation of satellite cells. The self-renewal of satellite cells is critical for long-term maintenance of muscle regeneration potential. Hypoxia profoundly affects the proliferation, differentiation, and self-renewal of cultured myoblasts. However, the physiological relevance of hypoxia and hypoxia signaling in satellite cells in vivo remains largely unknown. Here, we report that satellite cells are in an intrinsic hypoxic state in vivo and express hypoxia-inducible factor 2A (HIF2A). HIF2A promotes the stemness and long-term homeostatic maintenance of satellite cells by maintaining the quiescence, increasing the self-renewal and blocking the myogenic differentiation of satellite cells. HIF2A stabilization in satellite cells cultured under normoxia augmented their engraftment potential in regenerative muscle. Reversely, HIF2A ablation led to the depletion of satellite cells and the consequent regenerative failure in the long-term. In contrast, transient pharmacological inhibition of HIF2A accelerated muscle regeneration by increasing satellite cell proliferation and differentiation. Mechanistically, HIF2A induces the quiescence/self-renewal of satellite cells by binding the promoter of *Spry1* gene and activating *Spry1* expression. These findings suggest that HIF2A is a pivotal mediator of hypoxia signaling in satellite cells and may be therapeutically targeted to improve muscle regeneration.

## INTRODUCTION

The coordinated proliferation and differentiation of adult stem cells provide sustainable cell sources for tissue repair and regeneration. In support of long-term tissue homeostasis, many adult stem cell populations fine-tune the balance between proliferative and quiescent states so as to both meet the need for tissue repair and lessen cell cycle-associated stresses. Ineffective reversal of proliferation/quiescence in adult stem cells has been implicated in aging and many diseases (1).

Adult skeletal muscle stem cells, also called satellite cells (SCs), are essential for skeletal muscle regeneration (2). SCs and their undifferentiated progeny universally express Pax7, a character that has been utilized to identify both quiescent and proliferative SCs or manipulate gene expression specifically in SCs (3, 4). In uninjured muscle, SCs reside closely juxtaposed with contractile myofibers beneath the basal lamina and are mitotically quiescent. SC quiescence is jointly maintained by multiple mechanisms, but not limited to, TTP-mediated RNA decay, SIRT1-dependent histone deacetylation, restraint of myogenic and proliferation-associated gene expression by microRNAs (5-8). Upon muscle injury, SCs transit through a  $G_{(Alert)}$  phase and enter the cell cycle in response to the activation of HGF/FGF-mediated receptor tyrosine kinase (RTK) signaling and p38/MAPK signaling (9-11). After limited rounds of proliferation, a subset of SCs returns to quiescence and the niche location adjacent to myofibers (self-renewal), whereas many SCs undergo myogenic differentiation and eventually repair damaged myofibers. Angiopoietin-1/Tie2 RTK signaling, RTK negative regulator Spry1, and inactivation of p38/MAPK signaling promote SC self-renewal (11-13). Besides the above intrinsic mechanisms, dynamic remodeling of the muscle microenvironment also plays a critical role to

direct SC behaviors during muscle repair (2). However, how SCs fine-tune the scale of reversible quiescence and balance proliferation vs. differentiation remain incompletely understood.

Oxygen ( $O_2$ ) is essential for mitochondrial bioenergetics and energy homeostasis; low oxygen tension (hypoxia) underlies many disease conditions (14). The cellular responses to hypoxia are mainly mediated by hypoxia-inducible factors (HIFs), which form heterodimeric complexes between an  $O_2$ -sensitive alpha-subunit (HIF1A/HIF2A/HIF3A) and a stable beta-subunit (HIF1B)(15). Under normoxia, the alpha-subunit of HIF is hydroxylated and targeted to proteasome degradation. Under hypoxia, limited  $O_2$  stabilizes HIF complex, which binds hypoxia-responsive elements (HREs; 5'-RCGTG-3') and activates target gene expression. Many types of adult stem cells prefer hypoxic niches to maintain their quiescent and/or undifferentiated states (16). In vitro hypoxic conditions also profoundly impact the proliferation and differentiation of cultured SCs (myoblasts)(17). In addition, HIF1A knockout (KO) or compound HIF1A/HIF2A double KO in adult SCs distinctly affects SC numbers and muscle regeneration (18, 19). Yet, it remains elusive whether hypoxia is of any physiological relevance to SC in vivo, and if so, whether HIF-mediated hypoxia signaling regulates SC quiescence or can be potentially targeted to improve muscle regeneration.

Here, we demonstrated that SCs are inherently hypoxic within their in vivo niche. Quiescent SCs express HIF2A, but not HIF1A. HIF2A is essential for the maintenance of SCs in a quiescent and undifferentiated state and their long-term homeostasis in uninjured muscle. HIF2A stabilization promotes the self-renewal and stemness of normoxia-cultured SCs and improves their engraftment efficiency in a muscle injury model. Reversely, transient HIF2A inhibition shortly after muscle injury augments SC proliferation and myogenic differentiation and accelerates muscle regeneration and the recovery of contractile function. In SCs and myoblasts,

HIF2A transactivates the expression of *Spry1*, which has been shown as a negative regulator of RTK signaling and an essential factor for SC quiescence/self-renewal. Overall, this study identified HIF2A as a pivotal mediator of hypoxia signaling pathway in SCs and a promising therapeutic target for improving skeletal muscle repair.

## RESULTS

### Quiescent satellite cells are hypoxic in the niche and express HIF2A, but not HIF1A

The partial oxygen tension ( $pO_2$ ) of most adult tissues ranges 2~9% (20). To assess the intracellular  $pO_2$  of SCs in their niche, a hypoxia probe, pimonidazole, was administered in vivo, which forms protein adducts in hypoxic cells *in situ* (where  $pO_2 < 1.3\%$ )(21). Because the antibodies for SC marker Pax7 and pimonidazole are of the same isotype, pimonidazole was intraperitoneally injected to tamoxifen-treated adult *Pax7<sup>cre/ERT2</sup>;R26<sup>R</sup>CAG-Sun1/sfGFP* mice (hereafter called *SC-INTACT* mice; 3 mo. old), within which >99% Pax7<sup>pos</sup> quiescent SCs (QSCs) were genetically labeled with nuclear membrane-located GFP (nmGFP) in the muscle (Figure S1A-C)(22). On myofibers isolated from *extensor digitorum longus* (EDL) muscles, abundant pimonidazole adducts were detected in >99% nmGFP<sup>pos</sup> QSCs (particularly within the cytoplasm), indicating QSCs are in a hypoxic state in vivo (Figure 1A-B). The hypoxic state of QSCs was further confirmed by another hypoxia probe, CCI-103F. In adult wildtype *C57BL/6* mice, CCI-103F adducts were detected in the cytoplasm of ~97% Pax7<sup>pos</sup> QSCs (Figure 1C-D). In contrast to SCs, the sarcoplasm of myofibers or myonuclei stained little for pimonidazole/CCI-103F. Given this clear contrast, we investigated whether pimonidazole is capable of detecting hypoxia within myofibers. EDL myofibers from *SC-INTACT* mice were cultured *ex vivo* under hypoxia (1%  $pO_2$ ) and labeled with pimonidazole in the culture media

(Figure S1D). Under this defined hypoxic condition, pimonidazole adducts were detected in both cytoplasm and nuclei of SCs, in sarcoplasm of myofibers and at the periphery of myonuclei, but not within myonuclei (Figure S1E). Thus, QSCs are hypoxic in vivo, whereas the adjacent myofibers are likely not hypoxic. The non-hypoxic state of myofibers is consistent with the notion that the physiological  $pO_2$  of resting skeletal muscle is around 4.2% (23, 24).

Our previous RNA-seq analysis revealed abundant HIF1A and HIF2A mRNAs yet no HIF3A transcript in QSCs (25). To understand whether HIFs are stabilized in hypoxic QSCs, HIF1A and HIF2A were stained in uninjured resting muscles of adult *C57BL/6* mice (3 mo. old). HIF1A was not detected in most Pax7<sup>pos</sup> QSCs (Figure 1E, 1G, S1F); whereas ~90% QSCs had clear nuclear staining for HIF2A (Figure 1F, 1G, S1G). As hypoxia-stabilized HIFs function as transcription factors in the nucleus, the above observations indicate that HIF2A, not HIF1A, is selectively stabilized/expressed in hypoxic QSCs.

### **Muscle repair following eccentric contraction-induced injury is concomitant with dynamic alterations of HIF2A and HIF1A expression in satellite cells**

To assess the expression of HIFs in proliferative SCs during a physiological process of muscle repair, *tibialis anterior* (TA) and EDL muscles of adult *C57BL/6* mice were injured by eccentric contraction and the injured EDL myofibers were isolated from 1 to 9 days post-injury (dpi; Figure S2A). EdU and Evans Blue were administered 24-hrs before each myofiber isolation to assess cell proliferation and sarcolemma integrity, respectively. After the stretch-induced injury, Pax7<sup>pos</sup> SCs on injured EDL myofibers increased at 5 dpi, reached a peak at 7 dpi and declined from 7 to 9 dpi (Figure 2D), which is correlated with the repairing process as evidenced by the progressive restoration of sarcolemma integrity (Figure S2B). The dynamics of SC number is also correlated with the proliferative state of SCs (percents of EdU<sup>pos</sup> SCs), which

slightly increased at 1-2 dpi, peaked at 3 dpi and decreased from 3 to 9 dpi (Figure 2A, 2E). The expression of HIF2A in SCs altered during the repair process: at 1 dpi, ~80% SCs remained as HIF2A<sup>pos</sup>; from 2 to 5 dpi, only <10% SCs were HIF2A<sup>pos</sup>; HIF2A reappeared in ~60% SCs at 7 dpi and expressed in ~83% SCs at 9 dpi (Figure 2B, 2F). The dynamics of HIF2A expression and SC proliferation showed opposite trends (Pearson correlation coefficient = -0.71).

As HIF2A diminished in SCs from 1 to 2 dpi, we investigated whether hypoxia subsided in SCs at the same time. Pimonidazole was administered in stretch-injured SC-*INTACT* mice at 1, 2 and 3 dpi, when >90% nmGFP<sup>pos</sup> cells on injured EDL myofibers were still Pax7<sup>pos</sup> and remained as undifferentiated SCs (data not shown). At 1-3 dpi, pimonidazole was abundant in most nmGFP<sup>pos</sup> SCs, including those HIF2A<sup>neg</sup> SCs (at 2 and 3 dpi), indicating that SCs remained hypoxic when HIF2A diminished (Figure S2C-D).

The sustained hypoxia in SCs might be permissive for HIF1A stabilization. Indeed, discernible yet weak HIF1A staining was detected in ~7% Pax7<sup>pos</sup> SCs at 3 dpi, in ~43% SCs at 5 dpi, in ~20% SCs at 7 dpi, but was undetectable at 9 dpi (Figure 1C, 1G). The dynamics of HIF1A expression in SCs appeared to be positively correlated with SC proliferation (Pearson correlation coefficient = +0.42), corroborating the reported function of HIF1A in promoting SC proliferation under hypoxia (26).

### **Genetic ablation of HIF2A in QSCs leads to transient activation, proliferation, and differentiation of SCs**

Upon muscle injury, the robust SC proliferation following diminished HIF2A expression implicates a role of HIF2A in the maintenance of SC quiescence. To investigate this potential novel function of HIF2A, we administered tamoxifen in adult *Pax7<sup>cre/ERT2</sup>;HIF2A<sup>fllox/fllox</sup>* mice (hereafter called SC-*HIF2AKO* mice; 3 mo. old), which resulted in genetic ablation of HIF2A

specifically in SCs (Figure 3A-B). At 10 days post tamoxifen-induced recombination (10 dpr), HIF2A expression was abolished in ~80% SCs in uninjured EDL myofibers (Figure 3B-C). Myogenic transcription factor MyoD is absent in QSCs yet expressed in activated/proliferative SCs (27). HIF2A ablation led to a remarkable increase of MyoD<sup>pos</sup> SCs in uninjured myofibers (Figure 3B, 3D), suggesting HIF2A-depleted SCs were spontaneously activated in uninjured muscles.

To confirm that SCs proliferate after HIF2A ablation, we administered EdU in *SC-HIF2AKO* mice at 11-15 dpr (Figure 3E). At 16 dpr, uninjured TA muscles of *SC-HIF2AKO* mice contained increased numbers of Pax7<sup>pos</sup>/Ki67<sup>pos</sup> SCs and Pax7<sup>pos</sup>/EdU<sup>pos</sup> SCs, compared to the control (Figure 3F-H). Proliferation markers Ki67 and EdU were detected only in Pax7<sup>pos</sup> SCs, consistent with the specificity of HIF2A ablation in SC compartment (Figure 3F).

To investigate whether SCs differentiate following proliferation, we performed SC lineage tracing in *Pax7<sup>cre</sup>/ERT2;HIF2A<sup>flox/flox</sup>;R26R<sup>CAG-Sun1/sfGFP</sup>* mice (hereafter called *SC-HIF2AKO-INTACT* mice) and control *SC-INTACT* mice, wherein nmGFP-labeled SCs may remain as Pax7<sup>pos</sup> SCs or differentiate into Pax7<sup>neg</sup> myonuclei (Figure 3I-J). At 16 dpr, nmGFP<sup>pos</sup>/Pax7<sup>pos</sup> SCs increased in uninjured TA muscles of *SC-HIF2AKO-INTACT* mice, confirming SC proliferation upon HIF2A ablation; meanwhile, these uninjured/resting muscles also contained increased nmGFP<sup>pos</sup>/Pax7<sup>neg</sup> myonuclei, supporting massive myogenic differentiation of HIF2A-ablated SCs (Figure 3J-K). Myogenic transcription factor Myogenin is specifically expressed in differentiating myogenic cells (2). Uninjured EDL myofibers from *SC-HIF2AKO-INTACT* mice (16 dpr) contained increased number of nmGFP<sup>pos</sup>/Myogenin<sup>pos</sup> cells, compared to the control (Figure 3L, S3A), further confirming that HIF2A-ablation in SCs induces myogenic differentiation.

To investigate whether SC apoptosis follows HIF2A ablation, we performed TUNEL labeling on TA muscle sections from *SC-HIF2AKO-INTACT* and control *SC-INTACT* mice. For both types of mice, TUNEL<sup>+pos</sup> apoptotic nuclei counted for <0.5% of nmGFP<sup>+pos</sup> nuclei (of SCs and SC progeny) at 16 dpr (Figure S3B-C). In contrast, TUNEL<sup>+pos</sup> nuclei were readily detected in nuclease treated muscle sections (technical positive control; Figure S3D). Thus, SCs undergo activation/proliferation/differentiation, but not apoptosis, in uninjured/resting muscles after HIF2A ablation.

It has been previously reported that the depletion of one HIF alpha-subunit provokes the increase of the other (28). At 16 dpr, weak HIF1A expression was detected in about 15% Pax7<sup>+pos</sup> SCs on uninjured EDL myofibers from *SC-HIF2AKO* mice, but not in SCs from control (Figure S3E-F). As HIF2A expression is abolished in >90% SCs at 16 dpr (data not shown), HIF2A depletion seems not induce HIF1A compensation in the majority of SCs.

### **Long-term ablation of HIF2A results in the loss of SC homeostatic self-renewal**

The long-lasting regeneration capability of skeletal muscle depends on the self-renewal and homeostatic maintenance of SCs. We next investigated the impact of HIF2A ablation on SC self-renewal. Upon tamoxifen-induced HIF2A ablation, the number of Pax7<sup>+pos</sup> SC in TA muscles of *SC-HIF2AKO* mice increased to ~110% at 16 days, returned to the normal level at 1 month, and reduced to ~20% of the normal level at 6 months (Figure 4A-B), revealing that HIF2A ablation impaired SC self-renewal and the homeostatic maintenance. At 6 months after tamoxifen treatment, SC-depleted muscles in *SC-HIF2AKO* mice showed a discernible increase in myofiber calibers compared to the age-matched control (Figure 4C-D) yet with comparable maximal torques (Figure S3G). Therefore, HIF2A is essential for the quiescence and long-term homeostatic maintenance of SCs in adult uninjured muscle.

## **HIF2A stabilization under normoxia promotes quiescence, self-renewal and stemness of SCs yet impedes myogenic differentiation**

Hypoxia treatment increases the engraftment efficiency of cultured satellite cells (myoblasts) yet impairs their proliferation and differentiation (29, 30). The above phenotypes of HIF2A-ablated SCs intrigued us to investigate whether HIF2A-stabilization under normoxia is sufficient to elicit similar effects as hypoxia, which would be beneficial to SC transplantation-based therapy. After 72-hrs normoxic culture (21% pO<sub>2</sub>), SC clusters formed on myofibers due to the activation and proliferation of individual SCs. Unlike the nuclear localization of Pax7 and MyoD, HIF2A was detected in the cytoplasm of SCs, suggestive of its loss of function under normoxia (Figure S4A). The cytoplasmic staining is specific to HIF2A as evidenced by its absence in SC clusters derived from HIF2A-ablated SCs (16 dpr; Figure S4B). Similar to cultured SCs, C2C12 myoblasts cultured under normoxia also expressed a low but detectable level of HIF2A that was mainly present in the cytoplasmic fraction, in line with the notion that normoxia destabilizes HIF2A (Figure S4C).

To stabilize HIF2A in SCs under normoxia, we transfected cultured SCs with a plasmid expressing GFP (to trace transfection) and a triple mutated form of HIF2A (HIF2ATM, carrying P405A, P530V and N851A mutations of mouse HIF2A), which is resistant to oxygen-induced hydroxylation and proteasome degradation (Figure 5A)(31). After 72-hrs normoxic culture, control myofibers that were transfected only with GFP had 4.6 GFP<sup>pos</sup> SC clusters and 4.3 GFP<sup>pos</sup> SCs per cluster on average (Figure 5B-C). In contrast, myofibers that were transfected with HIF2ATM/GFP had markedly reduced number and size of GFP<sup>pos</sup> SC clusters (~1.9 clusters per myofiber and ~2.5 SCs per cluster on average; Figure 5B-C). Thus, HIF2A stabilization elicited opposite effects as HIF2A ablation, supporting HIF2A promotes SC

quiescence and impedes SC proliferation. In comparison, the transfection of a wildtype form of HIF2A (HIF2AWT) under normoxia did not alter the number and size of SC clusters (Figure S4D).

As a SC niche factor, myofibers in the above experiment were GFP<sup>pos</sup> and thus likely had altered HIF2A expression. Thus, we investigated whether HIF2A promote SC quiescence in a cell-autonomous manner. Transfection of HIF2ATM, but not HIF2AWT, in primary myoblasts under normoxia decreased the proliferation rate (Figure S4E, left). Cell cycle analysis revealed that HIF2ATM-transfection increased the percent of primary myoblasts in G0/G1 phases and decreased the percent of cells in G2/S phases (Figure S4F), indicating HIF2A stabilization in SCs is intrinsically sufficient to promote quiescence. In contrast to normoxic culture, primary myoblasts proliferated slowly under hypoxia (1% pO<sub>2</sub>) and HIF2ATM-transfection did not further repress the proliferation (Figure S4E, right). This corroborates with previous findings that hypoxia impairs myoblasts proliferation (17, 29) and implicates a role of HIF2A stabilization in this hypoxic effect.

To assess the impact of HIF2A stabilization on SC self-renewal and differentiation, we stained the normoxia-cultured SC clusters/myofibers for Pax7 and MyoD (Figure 5A-C). Compared to the control myofibers, HIF2ATM-transfected myofibers had increased numbers of Pax7<sup>pos</sup>/MyoD<sup>neg</sup> self-renewing SCs (HIF2ATM: 0.6 vs. control: 0.35 cells per cluster) yet decreased numbers of Pax7<sup>neg</sup>/MyoD<sup>pos</sup> committed myogenic SCs (HIF2ATM: 0.4 vs. control: 2.6 cells per cluster; Figure 5C). No such difference was observed after HIF2AWT transfection (Figure S4D). Thus, HIF2A stabilization promotes the self-renewal but impairs the myogenic differentiation of SCs.

To confirm the above effects are SC-autonomous, control and HIF2ATM-transfected C2C12 myoblasts were differentiated in 2% horse serum for 5 days (21% pO<sub>2</sub>) and stained for Pax7 and

myosin heavy chain (MyHC; Figure S4G). Myoblasts transfected with the control plasmid (GFP<sup>pos</sup>) were either Pax7<sup>pos</sup>/MyHC<sup>neg</sup> (self-renewed reserve cells) or Pax7<sup>neg</sup>/MyHC<sup>pos</sup> (differentiated myocytes). In contrast, cells transfected with HIF2ATM (GFP<sup>pos</sup>) were almost exclusively Pax7<sup>pos</sup>/MyHC<sup>neg</sup> (Figure S4G), confirming HIF2A intrinsically impedes myogenic differentiation but augments the self-renewal.

The above observations suggest that HIF2A stabilization may facilitate the engraftment efficiency of SCs after transplantation (remaining as stem cells). To assess this potential effect, we isolated myofibers (and residing SCs as donor cells) from *SC-INTACT* mice. The specific presence of nmGFP on SC nuclear membrane allowed us to trace the location and fates of transplanted SCs. The myofibers were transfected with control and HIF2ATM plasmids (no GFP expression) and transplanted into cardiotoxin (CTX)-injured TA muscles (1 dpi) of cognate *C57BL/6* host mice (3 mo. old; Figure 5D). As massive SC transplantation may alter muscle regeneration progression and hence indirectly affects SC fates, we only transplanted 10 myofibers (either control or HIF2A-transfected) into each injured TA muscle. Twenty-one days after transplantation, nmGFP<sup>pos</sup> nuclei were observed as Pax7<sup>neg</sup> differentiated myonuclei at the center of regenerated myofibers and in niche-residing Pax7<sup>pos</sup> self-renewed SCs (adjacent to basal lamina), representing two distinct fates of nmGFP<sup>pos</sup> donor SCs (Figure 5E). HIF2ATM-transfection increased the number of nmGFP<sup>pos</sup>/Pax7<sup>pos</sup> engrafted SCs (control: 2.2 SCs vs. HIF2A: 4.5 SCs per section; Figure S4H) and the percent of engrafted SCs in total Pax7<sup>pos</sup> SC pool (control: 2.5% vs. HIF2A: 4.8%; Figure 5F), indicating HIF2A improves SC engraftment efficiency. In contrast, HIF2ATM-transfection decreased the number of nmGFP<sup>pos</sup>/Pax7<sup>neg</sup> myonuclei (derived from nmGFP<sup>pos</sup> donor SCs; control: 43 nmGFP<sup>pos</sup> myonuclei vs. HIF2A: 32

nmGFP<sup>pos</sup> myonuclei; Figure 5G), which echoes the negative effect of HIF2A stabilization on myogenic differentiation in cultured SCs/myoblasts.

The long-term outcome of SC transplantation depends on a fine balance between the self-renewal and differentiation of engrafted SCs; either excessive self-renewal or unrestrained differentiation expectedly leads to a failure in support of repetitive muscle repair. Thus, we further investigated whether the skewed self-renewal/differentiation potential of HIF2A-stabilized SCs should eventually enhance the long-term engraftment of these stem cells and their contribution to muscle repair. To this aim, we injured the regenerated TA muscles that received SC engraftment (either control or HIF2ATM-transfected SCs) for the second time (Figure 5D). At 30 dpi, the TA muscles of both groups completed with regeneration and contained regenerated myofibers of comparable calibers (data not shown). Comparing to the control TA muscles, the TA muscles that originally engrafted HIF2ATM-transfected SCs contained markedly increased numbers of nmGFP<sup>pos</sup>/Pax7<sup>pos</sup> donor-originated SCs (control: 2.1 vs. HIF2A: 11.2 engrafted SCs per section; Figure S4I), which is consistent with the results of the first injury and further confirms HIF2A stabilization improves SC self-renewal. Comparing to the first round of regeneration, HIF2ATM-transfected SCs showed a markedly increased proportion in the total Pax7<sup>pos</sup> SC pool after the second regeneration (the first injury: 4.8% vs. the second injury: 11.6%; Figure 5F, 5H). This increase is likely due to superior self-renewal capabilities of HIF2ATM-transfected SCs compared to the endogenous SCs and implicates possible domination of these engrafted SCs in long-term repetitive muscle regeneration. Regarding the myogenic differentiation, the TA muscles that originally engrafted HIF2ATM-transfected SCs also contained increased numbers of nmGFP<sup>pos</sup>/Pax7<sup>neg</sup> donor-derived myonuclei at the end of the second round of regeneration (control: 61.3 vs. HIF2A: 76.5 nmGFP<sup>pos</sup> myonuclei; Figure

5l). Thus, although HIF2A<sup>TM</sup>-transfected SCs were twice as many as the control engrafted SCs (4.5/2.2=200%) at the beginning of the second regeneration, there was only a moderate increase of donor-derived myonuclei (76.5/61.3=124%). This likely reflects the negative impacts of HIF2A stabilization on SC proliferation and/or differentiation. However, the overall enhancement of the contribution to muscle regeneration and self-renewal potential suggests that HIF2A stabilization improves the long-term outcome of SC transplantation.

### **Genetic ablation of HIF2A transiently improves muscle regeneration but impairs long-term muscle regeneration potential**

As HIF2A ablation in QSCs led to transient SC proliferation and myogenic differentiation, we sought to understand whether these effects may improve muscle repair. Stretch-induced injury is of physiological relevance yet the diminished HIF2A expression in SCs after injury negates the necessity of genetic HIF2A ablation in this injury model. Unlike stretch-induced injury, HIF2A expression dampened but was still present in many SCs after CTX-induced injury (3 dpi; *C57BL/6* mice, 3 mo.; Figure S5A); meanwhile, most SCs (along with many Pax7<sup>-neg</sup> cells) expressed HIF1A, which is in line with reported massive blood vessel damage in CTX-injured muscles (Figure S5A)(32). Thus, we examined TA muscle regeneration following CTX-induced injury in *SC-HIF2AKO* mice and their control littermates, which were administered with tamoxifen at 8-10 days before CTX injury (to deplete HIF2A in SCs of *SC-HIF2AKO* mice). SC-specific HIF2A ablation increased the number of Pax7<sup>+pos</sup> SCs at 10 dpi in *SC-HIF2AKO* mice, compared to control (control: ~320 SCs vs. *SC-HIF2AKO*: ~420 SCs per TA section; Figure 6A-B), indicating HIF2A ablation transiently improves SC proliferation in regenerative muscle. Embryonic myosin heavy chain (eMyHC) was expressed at a higher level in newly formed/regenerating myofibers with centralized myonuclei in *SC-HIF2AKO* mice at 5 dpi,

suggesting HIF2A ablation also augments SC differentiation (Figure 6D). At 10 dpi, eMyHC already diminished in most myofibers in *SC-HIF2AKO* mice yet was still present in many myofibers of small calibers in the control mice, suggesting that regenerative myogenesis is accelerated in *SC-HIF2AKO* mice (Figure 6D). At 21 dpi, TA muscles of both *SC-HIF2AKO* and control mice contained fully regenerated myofibers (Figure 6D). The number of Pax7<sup>+</sup> SCs in *SC-HIF2AKO* mice was comparable to the control mice at 21 dpi, suggesting the decrease of SC self-renewal may be compensated by the increase of proliferation in regenerative muscles (Figure 6A, 6C). At 30 dpi, the percents of myofibers expressing myosin heavy chain isoforms I, IIA and IIB were comparable between *SC-HIF2AKO* and control mice (Figure S5B-C), indicating that SC-specific HIF2A ablation does not alter myofiber type composition during muscle regeneration.

Although HIF2A ablation in SCs transiently increases proliferation/myogenic differentiation and improves muscle regeneration, the depletion of SC pool after long-term HIF2A ablation expectedly impairs muscle regeneration instead. To confirm this, we injured TA muscles of *SC-HIF2AKO* and control mice with CTX at 6 months after tamoxifen-induced HIF2A ablation, when SCs exhausted in *SC-HIF2AKO* mice (Figure 4B). At 30 dpi, the injured TA muscles in control mice were completely regenerated, whereas only a small number of regenerated myofibers were observed in *SC-HIF2AKO* mice (Figure 6E). The distinct outcomes of muscle regeneration in *SC-HIF2AKO* mice echo the transient and long-term effects of HIF2A ablation in SCs, namely HIF2A ablation leads to transient increases of SC proliferation and myogenic differentiation, whereas HIF2A ablation in long-term eventually results in the loss of SC population and failure of regeneration.

## **Transient pharmacological inhibition of HIF2A in CTX-injured muscle promotes SC proliferation and accelerates muscle regeneration**

The above observations suggest that a transient HIF2A inhibition following hypoxia-burdened muscle injury may benefit regeneration by promoting SC proliferation yet lessening the side-effect of SC loss. To transiently inhibit HIF2A in muscle, we intramuscularly administered a HIF2A inhibitor (HIF-c2, CAS #:1422955-31-4; 5 mg/injection/day, 3 consecutive days), which reduced HIF2A expression in muscle (including SCs; Figure S6A) as previously reported (33). We administered HIF-c2 or the carrier solution (1% DMSO) into CTX-injured TA muscles of adult *C57BL/6* mice (daily injections on 1-3 dpi; Figure 7A). HIF-c2 treatment increased the number of Pax7<sup>+</sup>/EdU<sup>+</sup> proliferative SCs at 3 dpi and the number of Pax7<sup>+</sup> SCs at 7 dpi and 10 dpi (Figure 7B-D). At 7 dpi, HIF-c2-treated muscles contained regenerated myofibers of noticeably increased calibers and decreased expression of eMyHC (Figure 7E, S6B). Consistently, HIF-c2-treated muscles had reduced expression levels of HIF2A, proliferative SC marker MyoD and early regeneration marker eMyHC (Figure 7F). Additionally, HIF-c2-treated muscles recovered ~53% of the maximal torques measured before injury; whereas the control muscles only recovered ~32% of the maximal torques at 7 dpi (Figure 7H), indicating accelerated muscle regeneration. At 30 dpi, when muscle regeneration is completed, both HIF-c2-treated and control muscles contained comparable numbers of Pax7<sup>+</sup> SCs and recovered ~90% of the maximal torques (Figure 7D, 7H), suggesting the HIF-c2 treatment regimen does not affect SC self-renewal or future contractile capacity of regenerated muscle. However, regenerated myofibers in HIF-c2-treated muscles had increased myofiber calibers (Figure 7E, 7G). HIF-c2-treated muscles had no obvious sign of fibrosis and had similar myofiber

type composition as control muscles (Figure S6C-E). Therefore, transient inhibition of HIF2A after CTX-induced muscle injury accelerates the progression of muscle regeneration.

As HIF-c2 treatment is not specific to SCs, we asked whether the beneficial effects attribute to HIF2A inhibition in SCs. Thus, we repeated the same HIF-c2 treatment regimen (with 1% DMSO as control) in CTX-injured TA muscles from *SC-HIF2AKO* mice, wherein HIF2A had been genetically ablated in SCs (CTX injury at 10 dpr; Figure 7I). At 7 dpi, DMSO-treated muscles in *SC-HIF2AKO* mice had increased number of Pax7<sup>pos</sup> SCs compared to DMSO-treated muscles in the wildtype mice (Figure 7J, right). However, in *SC-HIF2AKO* mice, HIF-c2 treatment did not further increase the number of Pax7<sup>pos</sup> SCs at 7 dpi (compared to DMSO-treated *SC-HIF2AKO* mice; Figure 7J). In addition, eMyHC levels and the morphology of regenerating myofibers were comparable in HIF-c2 and DMSO-treated muscles of *SC-HIF2AKO* mice (Figure 7K). Thus, the beneficial effects of HIF-c2 on muscle regeneration in the wildtype mice are likely owing to HIF2A inhibition in SCs.

### ***Spry1* is a novel target of HIF2A in QSCs**

*Spry1* is highly expressed in QSCs but not in proliferative SCs and is essential for the self-renewal and maintenance of SCs (13, 34). Bioinformatic analysis identified three conserved HREs within the proximal promoter of *Spry1* gene (Figure S7A), suggesting that HIF2A promotes SC self-renewal by activating *Spry1*. In luciferase assays, the HRE-containing *Spry1* promoter was specifically responsive to stabilized HIF2A, but not stabilized HIF1A, in C2C12 myoblasts (Figure 8A). *Atp7a* and *Pdk3* are specific target genes of HIF2A and HIF1A, respectively (15, 35, 36). Consistently, an *Atp7a* promoter was specifically responsive to stabilized HIF2A, whereas a *Pdk3* promoter was only responsive to stabilized HIF1A.

To confirm HIF2A at its native expression level directly binds to the *Spry1* promoter under hypoxia, we performed HIF2A chromatin immunoprecipitation (ChIP) using  $2 \times 10^6$  nmGFP<sup>pos</sup> QSC nuclei that were fixed in vivo and isolated from *SC-INTACT* mice (Figure S7B and Methods). In support of the efficacy and specificity of HIF2A ChIP in QSCs, ChIP-qPCR revealed that a *Cav1* promoter, which was previously shown to associate with HIF2A in hypoxic colorectal epithelial cells (37), was also enriched for 3.4 folds in QSC HIF2A ChIP samples, whereas no enrichment was detected for the *Pdk3* promoter (Figure 8B). ChIP-qPCR also revealed ~13-fold of enrichment of the *Spry1* promoter in HIF2A ChIP samples, indicating HIF2A directly binds to the *Spry1* promoter in QSCs (Figure 8B).

To investigate whether HIF2A activates *Spry1* in QSCs, we isolated nmGFP<sup>pos</sup> SCs from *SC-INTACT* and *SC-INTACT-HIF2AKO* mice (at 10 dpr) by FACS and performed RT-qPCR. SCs from *SC-INTACT-HIF2AKO* mice had reduced expression of *Hif2a* and QSC markers, *Calcr* and *Cd36* (Figure 8C)(8, 38), confirming that HIF2A ablation leads to SC activation. Importantly, HIF2A-ablated SCs expressed decreased levels of *Spry1* and HIF2A targets, *Atp7a* and *Cxcl12* (Figure 8C)(39), indicating HIF2A transactivates *Spry1* (and *Atp7a*, *Cxcl12*) in SCs.

We further investigated whether *Spry1* expression is responsive to HIF2A expression levels in vitro. Under normoxia, two HIF2A-targeting shRNAs independently knockdowned *Hif2a* (but not *Hif1a*) in C2C12 myoblasts, which also decreased the expression of *Spry1*, *Atp7a*, and *Cxcl12* (Figure 8D, S7C). Similarly, HIF-c2, although not affecting *Hif2a* mRNA level, reduced HIF2A protein in C2C12 myoblasts as well as decreased the mRNA levels of *Spry1*, *Atp7a*, and *Cxcl12* (Figure 8E, S7D). Instead, HIF-c2 increased *Hif1a* mRNA, HIF1A protein, and mRNA levels of known HIF1A targets, *Pdk3* and *Slc2a1/Glut1* (Figure S7D-E)(40). Reversely, overexpressing HIF2ATM in C2C12 myoblasts increased mRNA levels of *Spry1*, *Atp7a*, and

*Cxcl12* (Figure 8F, S7F). Thus, *Spry1* is a novel HIF2A target gene and HIF2A transactivates *Spry1* in SCs and myoblasts.

## DISCUSSION

This study uncovers a previously unappreciated hypoxic state of SCs in their native niche. Pimonidazole and CCI-103F form non-specific protein adducts when  $pO_2$  is less than 1.3% (or 10 mmHg) and have been widely used to determine hypoxic states of stem cells and tumor cells in vivo (41-43). QSCs in healthy resting muscle stained positive for Pimonidazole and CCI-103F, indicating SCs are intracellularly hypoxic. This finding echoes a previous observation that SCs isolated from postmortem muscle retain the viability and regenerative potential (44) and implies that SCs are adapted to hypoxia. The  $pO_2$  in healthy resting muscle ranges from 3 to 4% (25-34 mmHg)(24, 45, 46). Consistently, we found that the sarcoplasm of myofibers stained much less for pimonidazole/CCI-103F. The distinct  $pO_2$  in SCs and myofibers is intriguing as these two types of cells are juxtaposed. It has been reported that SCs are preferentially localized adjacent to capillaries (47). Thus, the hypoxic state of SCs is likely not the result of poor oxygenation in their extracellular milieu, but rather due to an unknown intrinsic mechanism. Notably, hematopoietic stem cells in the bone marrow are also pimonidazole<sup>+pos</sup>, irrespective of variable distance to vasculature or local  $pO_2$  (1-4%), which are distinct from adjacent pimonidazole<sup>-neg</sup> cells (48, 49). Thus, a hypoxic state seems to be physiologically inherent to some adult stem cell populations, suggestive of an obligatory role of hypoxia in stem cell biology.

Mammalian cells sense and cope with hypoxia by stabilizing HIFs (HIF1A/HIF2A/HIF3A). In line with the hypoxic state, QSCs express HIF2A, but not HIF1A. This finding is novel but not surprising. Recent studies demonstrated that HIF1A and HIF2A, although share many common

targets, often have disparate or even opposite functions (50). Particularly, HIF1A promotes glucose uptake, augments glycolysis flux and reduces glucose oxidation in TCA cycle under hypoxia or pseudohypoxia, which favors biosynthesis and cell proliferation in many types of fast-cycling cells, such as hematopoietic stem cells and many types of cancer cells (50-52). In contrast, HIF2A promotes stem cell characteristics in multiple types of cancer stem cells and HIF2A re-expression suppresses the growth of soft tissue sarcoma (53-55). In addition, HIF2A enhances the stemness of human embryonic stem cells and the reprogramming efficiency of human induced pluripotent stem cells (15, 41). Thus, it is conceivable that the selective stabilization of HIF2A (but not HIF1A) in SCs ensures their quiescence and stemness. Indeed, HIF2A-ablated SCs proceed to proliferate, differentiate and eventually being exhausted in uninjured muscles, reflecting a pivotal role of HIF2A in the maintenance of this adult stem cell population.

This study also revealed intriguing expression patterns of HIF2A and HIF1A in SCs during muscle repair: after stretch muscle injury, HIF2A diminished in SCs, followed by SC proliferation and transient HIF1A expression in a subset of SCs; in contrast, after CTX-induced injury, most SCs expressed both HIF2A and HIF1A. The emerging HIF1A expression in SCs apparently correlates to vascular damage in muscle and local hypoxia/ischemia. In support of this view, it has been shown that HIF2A controls chronic hypoxia signaling under medium-level hypoxia, whereas HIF1A mediates acute hypoxia responses under transient extreme hypoxia (53, 54). However, it is notable that the above-mentioned HIF1A/HIF2A dynamics cannot be the sole result of HIF-alpha stabilization/destabilization in response to tissue oxygenation, as evidenced by 1) following HIF2A depletion, HIF1A emerged in a small percent of SCs in uninjured/resting muscles, wherein local  $pO_2$  likely remained unchanged; and 2) after stretch-induced muscle

injury, most SCs remained pimonidazole<sup>+pos</sup> yet HIF2A diminished. Instead, these observations strongly implicate O<sub>2</sub>-independent mechanisms in HIF1A/HIF2A regulation in SCs. Notably, the global translation profile of QSCs markedly differs from that of activated SCs (56) and the translation of *Hif2a* mRNA (but not *Hif1a* mRNA) is regulated by insulin receptor-PI3K-mTORC2 pathway and IREBP1 (57, 58). Thus, it is conceivable that HIF1A/HIF2A expression in SCs may be regulated at the translational level during muscle repair, which warrants further investigation in the future.

The SC-specific gain- and loss-of-function of HIF2A in this study derived consistent evidence, supporting HIF2A promotes SC quiescence or returning to quiescence (self-renewal), whereas impedes their myogenic differentiation. As self-renewal, proliferation, and differentiation divergently impact on SC number, HIF2A ablation led to distinct consequences in the aspect of the size of SC pool and muscle regeneration capacity. Shortly after HIF2A ablation, SCs transiently expanded in number and proceeded to myogenic differentiation, which benefits regeneration with increased inputs from the stem cell compartment. In contrast, chronic HIF2A loss in SCs skewed self-renewal vs. differentiation propensities and exhausted the stem cell pool, which was destructive to muscle regeneration.

Reduced stemness and the consequent poor long-term engraftment potential of in vitro expanded myoblasts presents one of the major hurdles towards SC-based cell therapies for degenerative muscle diseases (59). Myoblasts cultured under hypoxia have increased quiescence, self-renewal and engraftment efficiency (17). In this study, HIF2A stabilization/overexpression in normoxic culture elicited the same series of effects as hypoxia. Intriguingly, HIF2A-stabilized SCs outperformed the control transplanted SCs and the endogenous SCs in terms of the self-renewal capability and the overall contribution to the

myonucleus compartment after repetitive regeneration. It seems paradoxical that HIF2A promotes SC quiescence and also increases the number of engrafted SCs. It is also apparently conflicting that HIF2A impedes myogenic differentiation yet HIF2A-stabilized SCs gave rise to more myonuclei. However, it is notable that a small percent of SCs preferentially undergo asymmetric cell divisions, divide slowly and withdraw early from the cell cycle (11, 60-62). When transplanted, these SCs have long-term self-renewal ability and can efficiently regenerate injured muscles – characteristics of true stem cells (60). In this perspective, the above apparent conflicting observations may actually reflect the increased stemness in HIF2A-stabilized SCs characterized by the improved ability to maintain as quiescent/undifferentiated stem cells as well as to sustain a myogenic progenitor pool and support muscle regeneration in the long-term. Thus, compared to in vitro hypoxia treatment, HIF2A stabilization could afford lasting stemness enhancement and long-term engraftment of myoblasts in transplantation-based therapies for degenerative muscle diseases.

This study also revealed *Spry1* as a novel target of HIF2A in SCs. Like *Hif2a*, *Spry1* mRNA is abundant in QSCs and down-regulated in proliferative SCs and *Spry1* ablation in SCs results in a loss of SC quiescence in uninjured muscle and impaired SC self-renewal during muscle regeneration (13, 34). These resembled expression patterns and phenotypes suggest a genetic interaction between *Spry1* and HIF2A. In this study, strong evidence indicated that HIF2A binds to the *Spry1* promoter and transactivates *Spry1*. Interestingly, HIF1A appeared not to transactivate *Spry1*, which is in line with its absence in QSCs. Previous studies showed that HIF1A and HIF2A require distinct co-activators for transcriptional activation (63, 64). Further investigation of specific targets and co-activators of HIF1A and HIF2A in SCs would be instrumental to understand their distinct functions in SCs.

Various types of muscle injury involve different levels of vascular damage and expectedly have distinct impacts on HIF expression in SCs (32). We postulate that the vasculature in regenerative muscle coordinates with SCs via hypoxia signaling to meet distinct needs for SC proliferation upon different types of muscle injury. Understanding the hypoxia signaling in regenerative muscle may shed light on specific therapeutic strategies for muscle injuries complicated with different levels of hypoxia/ischemia. In this study, we demonstrated that HIF2A loss-of-function benefited muscle regeneration after CTX-induced injury, which involves vascular damage/remodeling and heterogeneous HIF2A reduction in activated SCs. HIF2A inhibition augmented SC proliferation and accelerates myogenic differentiation, apparently alleviated a negative impact of hypoxia/ischemia on muscle regeneration capacity. The beneficial effects of HIF2A inhibition are likely not the result of compensatory expression of HIF1A in that SC-specific HIF1A ablation has been shown to increase myogenic differentiation without an effect on SC expansion following ischemic muscle injury (18). Additionally, SC-specific ablation of both HIF-1 $\alpha$  and HIF-2 $\alpha$  impairs muscle regeneration with reduced SC expansion and self-renewal (19). A previous study reported that *Myogenin Cre*-mediated HIF2A ablation results in myofiber switching from slow to fast types (65). In addition, muscle regeneration with HIF1A ablation in SCs ends in muscle fibrosis (18). In this study, we did not observe these side-effects following transient HIF2A inhibition in regenerative muscle. Given the accelerated recovery of muscle contractile function, transient HIF2A inhibition represents an appealing strategy to improve muscle regeneration after hypoxia/ischemia-involved muscle injury.

## METHODS

### Animal experimental procedures

All animals were housed at 23°C with 12:12-hrs light:dark cycles with food/water *ad libitum*. All strains were purchased from the Jackson Laboratory: *Pax7<sup>creERT2</sup>* (#017763), *R26R<sup>CAG-Sun1/sfGFP</sup>* (#021039) and *Hif2a<sup>flox</sup>* (#008407).

To induce Cre activity, tamoxifen (20 mg/mL in corn oil) was intraperitoneally administered for 3 consecutive days (100 mg/kg/d). To assess myofiber damage, 1% Evans Blue (4 mL/kg in saline) was intraperitoneally administered. To trace proliferation, EdU (50 mg/kg in DMSO) was intraperitoneally administered. For induce muscle injury, CTX (0.5 nmol, 100 µL) was injected into TA muscle.

### Plasmid construction

For HIF1ATM/HIF2ATM expression, pcDNA3\_mHIF2A\_MYC and pcDNA3\_mHIF1A\_MYC plasmids were purchased from Addgene (#44027, #44028). HIF ORFs were sub-cloned into pCDH-CMV-MCS-EF1-eGFP-IRES-Puro plasmid (pCMEGIP; System Biosciences). For HIF2AWT expression, mHIF2A ORF was PCR amplified from a mouse cDNA library using the following primers:

HIF2A\_ORF\_S: 5'-ACAGCTGACAAGGAGAAAAAAGGAG-3'

HIF2A\_ORF\_AS: 5'-GGTGGCCTGGTCCAGAGC-3'

and cloned into the pCMEGIP plasmid.

For transplantation of HIF2ATM-transfected SCs/myofibers, the mHIF2ATM ORF was sub-cloned into pCDH-CMV-MCS-EF1-Puro plasmid (pCMEP; System Biosciences), which does not express GFP.

For HIF2A knockdown, HIF2A shRNA oligos (below) was cloned into pMSCV-P2GM plasmids (Addgene, #19750).

HIF2A shRNA #1 oligo

5'TGCTGTTGACAGTGAGCGAACACTTGATGTGGAAACGTATTAGTGAAGCCACAGATGTA  
ATACGTTTCCACATCAAGTGTGTGCCTACTGCCTCGGA-3'

HIF2A shRNA #2 oligo

5'TGCTGTTGACAGTGAGCGATCCAACAAGCTGAAGCTAAAGTAGTGAAGCCACAGATGTA  
CTTAGCTTCAGCTTGTTGGACTGCCTACTGCCTCGGA-3'

### ***In situ* detection of hypoxic SCs by hypoxypromes**

Hypoxypromes™-1 (pimonidazole, Hypoxypromes Inc.; 60 mg/kg in PBS) and Hypoxypromes™-F6 (CCI-103F, Hypoxypromes Inc.; 60 mg/kg in DMSO) were intraperitoneally administered at 1.5 and 3 hrs before euthanasia, respectively.

To assess Hypoxypromes™-1 in staining hypoxic myonuclei, myofibers from tamoxifen-induced *Pax7<sup>cre</sup>/ERT2;R26<sup>R</sup>CAG-Sun1/sfGFP* mice were cultured in a hypoxia chamber (Stem Cell Technologies) supplied with 1% O<sub>2</sub> and 5% CO<sub>2</sub> for 20 hrs and with the presence of Hypoxypromes™-1 (100 μM) for 2 hrs.

### **Maximal contraction force measurement and eccentric contraction-induced injury**

Peak isometric torque of the ankle dorsiflexors was assessed as previously described (66). Briefly, the left foot of anesthetized mice was placed on a foot plate attached to a servomotor (Model 300C-LR; Aurora Scientific). Two Pt-Ir electrode needles (Model E2-12; Grass Technologies) were inserted percutaneously on either side of the peroneal nerve. The ankle joint was secured at a 90° angle. Peak isometric torque was achieved by varying the current delivered

to the peroneal nerve at a frequency of 200 Hz and a 0.1-ms square wave pulse. Torques (N•mm) were normalized by the body mass ( $\text{kg}^{-1}$ ) to account for differences in body size.

To induce injury, the dorsiflexors were subject to 100 electronically stimulated eccentric contractions, during which the foot was passively moved from the  $0^\circ$  position (perpendicular to tibia) to  $20^\circ$  of dorsiflexion. The dorsiflexors were stimulated at 200 Hz for a 100-ms isometric contraction followed by an additional 50-ms stimulation while moving from  $20^\circ$  dorsiflexion to  $20^\circ$  plantarflexion at an angular velocity of  $800^\circ/\text{s}$ . Eccentric contractions were repeated every 10 s.

### **Myofiber isolation, culture, and transfection**

EDL myofibers were isolated as described before (67). Briefly, EDL was dissected and digested in 0.2% Type I Collagenase (Worthington) in DMEM at  $37^\circ\text{C}$  for 1.5 hrs. Single myofibers were isolated by triturating the digested EDL muscle with polished Pasteur pipettes. Myofibers were cultured in horse serum-coated 24-well plates in DMEM (4.5 g/L glucose) supplemented with 20% FBS, 1% sodium pyruvate and 1% chicken embryo-extract and 1% penicillin-streptomycin.

For myofiber transfection, myofibers were cultured for 12 hrs, transfected with 2  $\mu\text{g}$  plasmids with Lipofectamine™ 3000 (Thermo Fisher Scientific) for 6 hrs.

### **Satellite cell / myofiber transplantation**

Myofibers were isolated from tamoxifen-induced *Pax7<sup>cre/ERT2</sup>;R26R<sup>CAG-Sun1/sfGFP</sup>* (SC-*INTACT*) mice, cultured for 12 hrs, transfected with plasmids for 6 hrs, and briefly washed. Ten transfected myofibers were loaded into a 28-gauge insulin syringe and injected into each TA muscle that was damaged by CTX 24 hrs before.

### **Myoblast culture, transfection, and differentiation**

Primary myoblasts were isolated from 1-week old *C57BL/6* male mice as described before (68). Primary myoblasts were cultured on collagen-coated dishes in HAM's F10 medium supplemented with 20% FBS, 5  $\mu\text{g/L}$  basic FGF and 1% penicillin-streptomycin. C2C12 myoblasts were purchased from ATCC and cultured in DMEM (4.5 g/L glucose) medium supplemented with 10% FBS and 1% penicillin-streptomycin. For hypoxia treatment, primary myoblasts and C2C12 myoblasts were cultured in hypoxia chamber supplied with 1%  $\text{O}_2$  and 5%  $\text{CO}_2$ . C2C12 myoblasts were transfected with plasmids using TransIT-X2<sup>®</sup> (Mirus Bio). C2C12 myoblasts (100% confluency) were differentiated in DMEM (4.5 g/L glucose) medium supplemented with 2% horse serum for 5 days.

### **Cell cycle analysis of primary myoblasts**

Primary myoblasts were infected with lentivirus packaged from pCMEGIP-HIF2a<sup>TM</sup> plasmid or control pCMEGIP empty plasmid, selected with puromycin (0.5  $\mu\text{g/mL}$ ) for 1 week, fixed with 70% ethanol for 10 mins and stained with Hoechst 33342 (10  $\mu\text{g/mL}$ ). Myoblasts were run into a HyperCyAn cytometer (Beckman Coulter) and profiles were analyzed by FlowJo v10.

### **Fluorescence-activated cell sorting (FACS)**

SC sorting was performed on a MoFlo XDP sorter (Beckman Coulter). nmGFP<sup>+pos</sup> SCs ( $\sim 2 \times 10^5$ ) were FACS-sorted from 3 mo. old *SC-INTACT* and *SC-HIF2AKO-INTACT* mice (7 dpr) as previously described (68).

### **Immunofluorescence staining and imaging**

For staining muscle sections, muscle sections were fixed with paraformaldehyde (PFA)/PBS (1%, 10 mins), quenched with glycine (50 mM, 10 mins), permeabilized with Triton X-100 (0.5%, 10 mins), blocked with Mouse on Mouse Blocking Reagent (Vector Lab) and 5% BSA/5% normal goat serum/PBS and incubated with primary antibodies: anti-Pax7 (1:5; DSHB #Pax7), anti-

HIF2A (1:250; Novus Bio. #NB100-122), anti-HIF1A (1:250; Novus Bio. # NB100-105), anti-Ki67 (1:1,000; Abcam #ab15580), anti-Laminin B2 (1:1,000; Milipore #05-206), anti-embryonic MyHC (1:50, DSHB #F1.652), anti-MyHC type I, IIA, or IIB (1:50, DSHB #BA-D5, SC-71, BF-F3) overnight at 4°C. For EdU staining, Click-iT EdU Fluorescence Kit (Life Technologies) was used following the manufacturer's instruction before primary antibody application. Sections were washed in PBS/0.1% Tween-20, incubated with AlexaFluor-labeled secondary antibodies (1:200, 1 hr), washed and mounted with DAPI-containing mounting medium (Life technologies).

For staining myofibers and myoblasts, myofibers/myoblasts were fixed in PFA (4%, 10 mins), blocked in 5% BSA/5% normal goat serum/PBS, and incubated with primary antibodies: anti-Pax7 (1:50), anti-MyoD (1:250; Sigma #M6190), anti-HIF2A (1:250), anti-HIF1A (1:250), and anti-GFP (1:1,000; 101Bio #P601).

Mounted slides were imaged on a Zeiss LSM 710 confocal microscope.

### **TUNEL labeling**

Muscle sections were stained using FlowTACS™ Apoptosis Detection Kit (Thermo Fisher Scientific) following the manufacturer's instructions. Briefly, sections were fixed by formaldehyde (3.7%, 10 mins), washed with PBS, incubated with 20 µL Cytonin™ solution for 30 mins, and washed with PBS. At this step, sections assigned for positive controls were further incubated with 25 µL TACS-Nuclease solution at room temperature for 30 mins. All sections were washed with 1X Labeling Buffer, incubated with the labeling reaction mix (1 µL 50X MnCl<sub>2</sub>, 1 µL TdT dNTP mix, 1 µL TdT enzyme and 50 µL 1X Labeling Buffer) at room temperature for 1 hr, incubated with 1X Stop buffer, and washed by PBS. All sections were incubated with DAPI and streptavidin-AlexaFluor 647 (1:200) for 10 mins in the dark, washed and mounted for confocal microscopy.

## Sirius red staining

Muscle sections were stained with Sirius Red solution (0.1% in picric acid, 15 mins), washed with acetic acid (1%, 3 times) and mounted with Cytoseal™ 60 mounting medium (Thermo Fisher Scientific).

## Satellite cell nuclei isolation by isolation of nuclei tagged in specific cell types (INTACT)

*SC-INTACT* mice were administered with tamoxifen 1 week before nuclei isolation to induce sfGFP- and myc-tagged Sun1 localization on SC nuclear membrane. 2.5 µg anti-GFP (101Bio #P601) and 2.5 µg anti-Myc (Millipore #05-419) antibodies were incubated with Protein A Dynabeads® (50 µL 50% slurry) in PBST on a rotating platform at 4°C overnight. To crosslink HIF2A *in situ* on chromatin of SCs *in vivo*, *SC-INTACT* mice were transcardially perfused with 30 mL 0.5% PFA and 30 mL 125 mM glycine as previously described (69). Limb and trunk muscles were dissected, ground in a mortar with liquid nitrogen, and homogenized (15 mL Wheaton dounce, loose pestle) in homogenization buffer (250 mM sucrose, 2 mM MgCl<sub>2</sub>, 25 mM KCl, 1% NP40) for 30 strokes. The homogenate was filtered by 100 µm and 40 µm strainers and centrifuged at 1,000 xg, 4°C for 5 min to collect crude nuclei. Nuclei were resuspended in 10 mL homogenization buffer and loaded on top of a two-step buffer cushion (lower buffer: 500 mM sucrose, 2 mM MgCl<sub>2</sub>, 25 mM KCl and 40% glycerol; upper buffer: 340 mM sucrose, 2 mM MgCl<sub>2</sub>, 25 mM KCl and 40% glycerol). The nuclei were centrifuged in a swing bucket rotor at 1,000 xg, 4°C for 10 min. Nuclei enriched at the interface were collected by long-neck Pasteur pipettes and checked under a fluorescent microscope. The above homogenization/centrifugation procedure was repeated until most nmGFP<sup>pos</sup> SC nuclei were physically separated from tissue debris or other nmGFP<sup>neg</sup> nuclei. Nuclei were incubated with antibody-coated Dynabeads in INTACT IP buffer (340 mM sucrose, 2 mM MgCl<sub>2</sub>, 25 mM KCl and 5% glycerol) on a rotating

platform (8 rpm/min) at 4°C for overnight. Nuclei tethered on Dynabeads were isolated on magnetic stands and washed (~6 times) with PBS to remove the non-bound nmGFP<sup>-neg</sup> nuclei. After each round of washing, the yield and purity of nmGFP<sup>+pos</sup> SC nuclei were assessed under a microscope.

### **Chromatin immunoprecipitation (ChIP) and ChIP-qPCR**

INTACT-purified SC nuclei (with Dynabeads) were resuspended in 100 µL lysis buffer (1% SDS, 10 mM EDTA, 50 mM Tris·HCl pH 8.1, 1x protease inhibitor cocktail) and sonicated at 4°C in a Bioruptor® Pico sonicator (Diagenode) using 15 on/off cycles of 30:30 seconds. The sheared chromatin (~300 bp) was 1:10 diluted in IP dilution buffer (50 mM HEPES-KOH pH7.5, 140 mM NaCl, 1 mM EDTA, 1% Triton X-100, 0.1% sodium deoxycholate, 0.1% SDS) and centrifuged at 20,000 xg, 4°C for 10 min. The supernatant was transferred to siliconized tubes and incubated with 2 µg HIF2A antibody (Novus Bio.) or rabbit IgG (Santa Cruz) on a rotating platform at 4°C overnight. PBS-washed Protein A Dynabeads® (30 µL 50% slurry) were added to the chromatin/antibody mix and incubated on a rotating platform at 4°C for 4 hrs. All ChIP beads were sequentially washed with low salt, high salt, lithium and TE buffer for 2 times/each and reverse-crosslinked with 1M NaCl for 6 hrs at 65°C. Samples were digested with 10 µg RNase A (37°C, 0.5 hr) and 20 µg Proteinase K (55°C, overnight). ChIPed gDNA was purified by phenol/chloroform/isoamyl alcohol (25:24:1) extraction followed by precipitation with 100% isopropanol, 0.3 M sodium acetate and GlycolBlue at -20°C overnight. The following primers were used to quantify relative enrichment levels at HRE-flanking regions in promoters of *Spry1*, *Cav1* and *Pdk3* genes in mouse genome:

Spry1\_promoter\_S: 5'-GAGTGTCCTGGGTTCTTGC-3'

Spry1\_promoter\_AS: 5'-GGCATAATGCATTTGCAAGC-3'

Cav1\_promoter\_S: 5'-CCTTGGGGATGTGCCTAG-3'  
Cav1\_promoter\_AS: 5'-CAGGGGTTTGTCTGCTCT-3'  
Pdk3\_promoter\_S: 5'- CCGCGACACCTACACAAG-3'  
Pdk3\_promoter\_AS: 5'- TTACCGGGGCTTTAAGGAAG-3'

The following primers were used for PCR amplification of gene-lacking regions on chromosome 5 and 6, which serve as inner reference controls in the calculation of relative enrichment levels:

Chr5\_S: 5'-CCCGTCACTCAACCATTTCA-3'  
Chr5\_AS: 5'-CTTATCAATGGGGGCTCTGG-3'  
Chr6\_S: 5'-AGATATGGCTGGCTTTGTGC-3'  
Chr6\_AS: 5'-GAACTCGCTCAGGTTCTGC-3'

#### **RT-qPCR**

Total RNA was isolated from C2C12 myoblasts using TRIzol or from FACS-sorted SCs using PicoPure RNA Isolation Kit (Thermo Fisher Scientific). Total RNA (1 µg from C2C12 myoblasts, or 0.2 µg from SCs) was used in 20 µL reverse transcription reactions (Maxima; Life technologies) and 1:5 diluted. qPCR reactions were performed with SsoAdvanced™ Universal SYBR Green mix (Bio-Rad) on a BioRad CFX384™ PCR system. Relative expression values (normalized to *Rps18* and *Tbp*) were calculated by BioRad CFX Manager™ Software. The following primers were used for RT-qPCR:

HIF2A\_S 5'-ACATGGCCCCCGATGAAT-3'  
HIF2A\_AS 5'-CAGGTAAGGCTCGAACGATG-3'  
HIF1A\_S 5'-ATAGCTTCGCAGAATGCTCAG-3'  
HIF1A\_AS 5'-CAGTCACCTGGTTGCTGCAA-3'  
Spry1\_S 5'-GGATTTGGCCGAGAGTTGTT-3'  
Spry1\_AS 5'-CGGCTAGGAGAAGGACACTA-3'  
Atp7a\_S 5'-AAAGAAGAGGTTCGGACTGCT-3'

Atp7a_AS	5'-AATGCCAACCTGAGAAGCAAT-3'
Cxcl12_S	5'-TGCATCAGTGACGGTAAACC-3'
Cxcl12_AS	5'-TGGGCTGTTGTGCTTACTTG-3'
Slc2a1_S	5'-CAGTTCGGCTATAAACTGGTG-3'
Slc2a1_AS	5'-GCCCCCGACAGAGAAGATG-3'
Calcr_S	5'-CGGCGGGATCCTATAAGTTG-3'
Calcr_AS	5'-GCGTGGATAATGGTTGGCA-3'
Cd36_S	5'-TCCTCTGACATTTGCAGGTC-3'
Cd36_AS	5'-AAGGCATTGGCTGGAAGA-3'
Rps18_S	5'-CGCCATGTCTCTAGTGATCC-3'
Rps18_AS	5'-GGTCGATGTCTGCTTTCCTC-3'
Tbp_S	5'-ACTTCGTGCAAGAAATGCTGA-3'
Tbp_AS	5'-TCTGGATTGTTCTTCACTCTTGG-3'

### Immunoblotting

Whole cell lysates were prepared by lysing cells in RIPA buffer supplemented with 1x proteinase inhibitor cocktail. Protein concentration was quantified by BCA Protein Assays (Thermo Fisher Scientific). Membrane was blocked with 5% non-fat milk/TBST, probed with primary antibodies: anti-HIF2A (1:1,000), anti-HIF1A (1:1,000), anti-HA tag (1:10,000; Thermo Fisher Scientific #26183) and anti-alpha-Tubulin (1:5,000; Sigma # T6199), incubated with ECL reagents (Santa Cruz) and exposed to X-ray films.

### Luciferase assay

A *Spry1* promoter region (-341 to +39 bp relative to TSS) and a *Pdk3* promoter region (-107 to +101 bp relative to TSS) were PCR amplified from genomic DNA (*C57BL/6* male) and cloned into pGL4.18 (Promega). pGL4.18\_ *Atp7a* has been reported before (35). pGL4.18-*Spry1*, pGL4.18-*Atp7a*, pGL4.18-*Pdk3* (200 ng/each) were co-transfected with pcDNA3-HIF1ATM, pcDNA3-HIF2ATM or control empty pcDNA3 plasmid (200 ng) into C2C12 myoblasts. pcDNA-LacZ (100 ng) expressing  $\beta$ -gal was co-transfected as an internal transfection control. At 48 hrs

post transfection, myoblasts were lysate with Luciferase Cell Lysis Buffer (NEB), followed by firefly luciferase/ $\beta$ -gal assay with homemade luciferase and  $\beta$ -gal solutions. Luciferase assay solution: 0.11M Trizma pH7.8, 0.5M  $MgCl_2$ , 0.1M ATP and 10mM Luciferin.  $\beta$ -gal solution: 4 mg/ml o-nitrophenyl-  $\beta$ -D-galactoside, 60 mM  $Na_2HPO_4$ , 40 mM  $NaH_2PO_4$ , 10 mM KCl, and 1 mM  $MgSO_4$ .

### **Statistics**

All values in the figures represent mean  $\pm$  s.e.m with  $\geq 3$  biological replicates. Statistical significance was determined by Prism GraphPad 6 using Student's *t*-test (two-sided). \*:  $p < 0.05$ , \*\*:  $p < 0.01$ , \*\*\*:  $p < 0.005$ , n.s.: not significant ( $p \geq 0.05$ ).

### **Study approval**

All animal studies were approved by the University of Georgia Institutional Animal Care and Use Committee (IACUC) and performed strictly following the guidelines.

### **AUTHOR CONTRIBUTIONS**

Conceptualization, H.Y.; Methodology, L.X., A.Y., A.M.B., J.A.C. and H.Y.; Investigation, L.X., A.Y., A.S.N., A.M.B., J.A.C. and H.Y.; Writing – Original Draft, H.Y.; Writing – Review & Editing, L.X., A.Y., A.M.B., J.A.C. and H.Y.; Funding Acquisition, H.Y.; Resources, A.M.B., J.A.C. and H.Y.; Supervision, H.Y.

### **ACKNOWLEDGEMENTS**

We thank Yang Liu of Yin laboratory for cloning and preparing pMSCV-P2GM-HIF2A shRNA constructs, Julie Nelson of UGA CTEGD Cytometry laboratory for help in FACS and Heather Flanagan-Steet for providing training on confocal microscopy. Research reported in this

publication was supported by the National Institute of Arthritis and Musculoskeletal and Skin Diseases of the National Institutes of Health under award number 1R01AR070178-01 to HY and American Heart Association postdoctoral fellowship under award number 16POST26400005 to L.X. The content is solely the responsibility of the authors and does not necessarily represent the official views of the National Institutes of Health or American Heart Association.

## REFERENCES

1. Goodell MA, and Rando TA. Stem cells and healthy aging. *Science*. 2015;350(6265):1199-204.
2. Yin H, Price F, and Rudnicki MA. Satellite cells and the muscle stem cell niche. *Physiological reviews*. 2013;93(1):23-67.
3. Murphy MM, Lawson JA, Mathew SJ, Hutcheson DA, and Kardon G. Satellite cells, connective tissue fibroblasts and their interactions are crucial for muscle regeneration. *Development*. 2011;138(17):3625-37.
4. Seale P, Sabourin LA, Girgis-Gabardo A, Mansouri A, Gruss P, and Rudnicki MA. Pax7 is required for the specification of myogenic satellite cells. *Cell*. 2000;102(6):777-86.
5. Cheung TH, Quach NL, Charville GW, Liu L, Park L, Edalati A, et al. Maintenance of muscle stem-cell quiescence by microRNA-489. *Nature*. 2012;482(7386):524-8.
6. Crist CG, Montarras D, and Buckingham M. Muscle satellite cells are primed for myogenesis but maintain quiescence with sequestration of Myf5 mRNA targeted by microRNA-31 in mRNP granules. *Cell Stem Cell*. 2012;11(1):118-26.
7. Hausburg MA, Doles JD, Clement SL, Cadwallader AB, Hall MN, Blackshear PJ, et al. Post-transcriptional regulation of satellite cell quiescence by TTP-mediated mRNA decay. *Elife*. 2015;4:e03390.
8. Ryall JG, Dell'Orso S, Derfoul A, Juan A, Zare H, Feng X, et al. The NAD(+)-dependent SIRT1 deacetylase translates a metabolic switch into regulatory epigenetics in skeletal muscle stem cells. *Cell Stem Cell*. 2015;16(2):171-83.
9. Rodgers JT, King KY, Brett JO, Cromie MJ, Charville GW, Maguire KK, et al. mTORC1 controls the adaptive transition of quiescent stem cells from G0 to G(Alert). *Nature*. 2014;510(7505):393-6.
10. Jones NC, Tyner KJ, Nibarger L, Stanley HM, Cornelison DD, Fedorov YV, et al. The p38alpha/beta MAPK functions as a molecular switch to activate the quiescent satellite cell. *J Cell Biol*. 2005;169(1):105-16.
11. Troy A, Cadwallader AB, Fedorov Y, Tyner K, Tanaka KK, and Olwin BB. Coordination of satellite cell activation and self-renewal by Par-complex-dependent asymmetric activation of p38alpha/beta MAPK. *Cell Stem Cell*. 2012;11(4):541-53.
12. Abou-Khalil R, Le Grand F, Pallafacchina G, Valable S, Authier FJ, Rudnicki MA, et al. Autocrine and paracrine angiopoietin 1/Tie-2 signaling promotes muscle satellite cell self-renewal. *Cell Stem Cell*. 2009;5(3):298-309.

13. Shea KL, Xiang W, LaPorta VS, Licht JD, Keller C, Basson MA, et al. Sprouty1 regulates reversible quiescence of a self-renewing adult muscle stem cell pool during regeneration. *Cell Stem Cell*. 2010;6(2):117-29.
14. Semenza GL. Hypoxia-inducible factors in physiology and medicine. *Cell*. 2012;148(3):399-408.
15. Mathieu J, Zhou W, Xing Y, Sperber H, Ferreccio A, Agoston Z, et al. Hypoxia-inducible factors have distinct and stage-specific roles during reprogramming of human cells to pluripotency. *Cell Stem Cell*. 2014;14(5):592-605.
16. Mohyeldin A, Garzon-Muvdi T, and Quinones-Hinojosa A. Oxygen in stem cell biology: a critical component of the stem cell niche. *Cell Stem Cell*. 2010;7(2):150-61.
17. Chaillou T, and Lanner JT. Regulation of myogenesis and skeletal muscle regeneration: effects of oxygen levels on satellite cell activity. *FASEB J*. 2016;30(12):3929-41.
18. Majmundar AJ, Lee DS, Skuli N, Mesquita RC, Kim MN, Yodh AG, et al. HIF modulation of Wnt signaling regulates skeletal myogenesis in vivo. *Development*. 2015;142(14):2405-12.
19. Yang X, Yang S, Wang C, and Kuang S. The hypoxia-inducible factors HIF1alpha and HIF2alpha are dispensable for embryonic muscle development but essential for postnatal muscle regeneration. *J Biol Chem*. 2017;292(14):5981-91.
20. Brahimi-Horn MC, and Pouyssegur J. Oxygen, a source of life and stress. *FEBS Lett*. 2007;581(19):3582-91.
21. Chou SC, Azuma Y, Varia MA, and Raleigh JA. Evidence that involucrin, a marker for differentiation, is oxygen regulated in human squamous cell carcinomas. *Br J Cancer*. 2004;90(3):728-35.
22. Deal RB, and Henikoff S. A simple method for gene expression and chromatin profiling of individual cell types within a tissue. *Dev Cell*. 2010;18(6):1030-40.
23. Beerthuizen GI, Goris RJ, and Kreuzer FJ. Skeletal muscle Po<sub>2</sub> during imminent shock. *Arch Emerg Med*. 1989;6(3):172-82.
24. Richardson RS, Duteil S, Wary C, Wray DW, Hoff J, and Carrier PG. Human skeletal muscle intracellular oxygenation: the impact of ambient oxygen availability. *J Physiol*. 2006;571(Pt 2):415-24.
25. Yin H, Pasut A, Soleimani VD, Bentzinger CF, Antoun G, Thorn S, et al. MicroRNA-133 controls brown adipose determination in skeletal muscle satellite cells by targeting Prdm16. *Cell metabolism*. 2013;17(2):210-24.

26. Ren H, Accili D, and Duan C. Hypoxia converts the myogenic action of insulin-like growth factors into mitogenic action by differentially regulating multiple signaling pathways. *Proc Natl Acad Sci U S A*. 2010;107(13):5857-62.
27. Zammit PS, Golding JP, Nagata Y, Hudon V, Partridge TA, and Beauchamp JR. Muscle satellite cells adopt divergent fates: a mechanism for self-renewal? *J Cell Biol*. 2004;166(3):347-57.
28. Menrad H, Werno C, Schmid T, Copanaki E, Deller T, Dehne N, et al. Roles of hypoxia-inducible factor-1alpha (HIF-1alpha) versus HIF-2alpha in the survival of hepatocellular tumor spheroids. *Hepatology*. 2010;51(6):2183-92.
29. Liu W, Wen Y, Bi P, Lai X, Liu XS, Liu X, et al. Hypoxia promotes satellite cell self-renewal and enhances the efficiency of myoblast transplantation. *Development*. 2012;139(16):2857-65.
30. Majmundar AJ, Skuli N, Mesquita RC, Kim MN, Yodh AG, Nguyen-McCarty M, et al. O(2) regulates skeletal muscle progenitor differentiation through phosphatidylinositol 3-kinase/AKT signaling. *Mol Cell Biol*. 2012;32(1):36-49.
31. Hu CJ, Sataur A, Wang L, Chen H, and Simon MC. The N-terminal transactivation domain confers target gene specificity of hypoxia-inducible factors HIF-1alpha and HIF-2alpha. *Mol Biol Cell*. 2007;18(11):4528-42.
32. Hardy D, Besnard A, Latil M, Jouvion G, Briand D, Thepenier C, et al. Comparative Study of Injury Models for Studying Muscle Regeneration in Mice. *PLoS One*. 2016;11(1):e0147198.
33. Scheuermann TH, Li Q, Ma HW, Key J, Zhang L, Chen R, et al. Allosteric inhibition of hypoxia inducible factor-2 with small molecules. *Nat Chem Biol*. 2013;9(4):271-6.
34. Chakkalakal JV, Jones KM, Basson MA, and Brack AS. The aged niche disrupts muscle stem cell quiescence. *Nature*. 2012;490(7420):355-60.
35. Xie L, and Collins JF. Transcriptional regulation of the Menkes copper ATPase (*Atp7a*) gene by hypoxia-inducible factor (HIF2{alpha}) in intestinal epithelial cells. *Am J Physiol Cell Physiol*. 2011;300(6):C1298-305.
36. Lu CW, Lin SC, Chen KF, Lai YY, and Tsai SJ. Induction of pyruvate dehydrogenase kinase-3 by hypoxia-inducible factor-1 promotes metabolic switch and drug resistance. *J Biol Chem*. 2008;283(42):28106-14.
37. Xie L, Xue X, Taylor M, Ramakrishnan SK, Nagaoka K, Hao C, et al. Hypoxia-inducible factor/MAZ-dependent induction of caveolin-1 regulates colon permeability through suppression of occludin, leading to hypoxia-induced inflammation. *Mol Cell Biol*. 2014;34(16):3013-23.

38. Yamaguchi M, Watanabe Y, Ohtani T, Uezumi A, Mikami N, Nakamura M, et al. Calcitonin Receptor Signaling Inhibits Muscle Stem Cells from Escaping the Quiescent State and the Niche. *Cell Rep.* 2015;13(2):302-14.
39. Martin SK, Diamond P, Williams SA, To LB, Peet DJ, Fujii N, et al. Hypoxia-inducible factor-2 is a novel regulator of aberrant CXCL12 expression in multiple myeloma plasma cells. *Haematologica.* 2010;95(5):776-84.
40. Hu CJ, Wang LY, Chodosh LA, Keith B, and Simon MC. Differential roles of hypoxia-inducible factor 1alpha (HIF-1alpha) and HIF-2alpha in hypoxic gene regulation. *Mol Cell Biol.* 2003;23(24):9361-74.
41. Das B, Bayat-Mokhtari R, Tsui M, Lotfi S, Tsuchida R, Felsher DW, et al. HIF-2alpha suppresses p53 to enhance the stemness and regenerative potential of human embryonic stem cells. *Stem Cells.* 2012;30(8):1685-95.
42. Parmar K, Mauch P, Vergilio JA, Sackstein R, and Down JD. Distribution of hematopoietic stem cells in the bone marrow according to regional hypoxia. *Proc Natl Acad Sci U S A.* 2007;104(13):5431-6.
43. Kizaka-Kondoh S, and Konse-Nagasawa H. Significance of nitroimidazole compounds and hypoxia-inducible factor-1 for imaging tumor hypoxia. *Cancer Sci.* 2009;100(8):1366-73.
44. Latil M, Rocheteau P, Chatre L, Sanulli S, Memet S, Ricchetti M, et al. Skeletal muscle stem cells adopt a dormant cell state post mortem and retain regenerative capacity. *Nat Commun.* 2012;3:903.
45. Boekstegers P, Riessen R, and Seyde W. Oxygen partial pressure distribution within skeletal muscle: indicator of whole body oxygen delivery in patients? *Adv Exp Med Biol.* 1990;277:507-14.
46. Ikossi DG, Knudson MM, Morabito DJ, Cohen MJ, Wan JJ, Khaw L, et al. Continuous muscle tissue oxygenation in critically injured patients: a prospective observational study. *J Trauma.* 2006;61(4):780-8; discussion 8-90.
47. Christov C, Chretien F, Abou-Khalil R, Bassez G, Vallet G, Authier FJ, et al. Muscle satellite cells and endothelial cells: close neighbors and privileged partners. *Mol Biol Cell.* 2007;18(4):1397-409.
48. Nombela-Arrieta C, Pivarnik G, Winkel B, Canty KJ, Harley B, Mahoney JE, et al. Quantitative imaging of haematopoietic stem and progenitor cell localization and hypoxic status in the bone marrow microenvironment. *Nat Cell Biol.* 2013;15(5):533-43.
49. Spencer JA, Ferraro F, Roussakis E, Klein A, Wu J, Runnels JM, et al. Direct measurement of local oxygen concentration in the bone marrow of live animals. *Nature.* 2014;508(7495):269-73.

50. Keith B, Johnson RS, and Simon MC. HIF1alpha and HIF2alpha: sibling rivalry in hypoxic tumour growth and progression. *Nat Rev Cancer*. 2011;12(1):9-22.
51. Xie H, and Simon MC. Oxygen availability and metabolic reprogramming in cancer. *J Biol Chem*. 2017;292(41):16825-32.
52. Nakazawa MS, Keith B, and Simon MC. Oxygen availability and metabolic adaptations. *Nat Rev Cancer*. 2016;16(10):663-73.
53. Holmquist-Mengelbier L, Fredlund E, Lofstedt T, Noguera R, Navarro S, Nilsson H, et al. Recruitment of HIF-1alpha and HIF-2alpha to common target genes is differentially regulated in neuroblastoma: HIF-2alpha promotes an aggressive phenotype. *Cancer Cell*. 2006;10(5):413-23.
54. Koh MY, Lemos R, Jr., Liu X, and Powis G. The hypoxia-associated factor switches cells from HIF-1alpha- to HIF-2alpha-dependent signaling promoting stem cell characteristics, aggressive tumor growth and invasion. *Cancer Res*. 2011;71(11):4015-27.
55. Nakazawa MS, Eisinger-Mathason TS, Sadri N, Ochocki JD, Gade TP, Amin RK, et al. Epigenetic re-expression of HIF-2alpha suppresses soft tissue sarcoma growth. *Nat Commun*. 2016;7:10539.
56. Zismanov V, Chichkov V, Colangelo V, Jamet S, Wang S, Syme A, et al. Phosphorylation of eIF2alpha Is a Translational Control Mechanism Regulating Muscle Stem Cell Quiescence and Self-Renewal. *Cell Stem Cell*. 2016;18(1):79-90.
57. Mohlin S, Hamidian A, von Stedingk K, Bridges E, Wigerup C, Bexell D, et al. PI3K-mTORC2 but not PI3K-mTORC1 regulates transcription of HIF2A/EPAS1 and vascularization in neuroblastoma. *Cancer Res*. 2015;75(21):4617-28.
58. Toschi A, Lee E, Gadir N, Ohh M, and Foster DA. Differential dependence of hypoxia-inducible factors 1 alpha and 2 alpha on mTORC1 and mTORC2. *J Biol Chem*. 2008;283(50):34495-9.
59. Briggs D, and Morgan JE. Recent progress in satellite cell/myoblast engraftment -- relevance for therapy. *FEBS J*. 2013;280(17):4281-93.
60. Ono Y, Masuda S, Nam HS, Benezra R, Miyagoe-Suzuki Y, and Takeda S. Slow-dividing satellite cells retain long-term self-renewal ability in adult muscle. *J Cell Sci*. 2012;125(Pt 5):1309-17.
61. Rocheteau P, Gayraud-Morel B, Siegl-Cachedenier I, Blasco MA, and Tajbakhsh S. A subpopulation of adult skeletal muscle stem cells retains all template DNA strands after cell division. *Cell*. 2012;148(1-2):112-25.
62. Kuang S, Kuroda K, Le Grand F, and Rudnicki MA. Asymmetric self-renewal and commitment of satellite stem cells in muscle. *Cell*. 2007;129(5):999-1010.

63. Chen Z, Liu X, Mei Z, Wang Z, and Xiao W. EAF2 suppresses hypoxia-induced factor 1alpha transcriptional activity by disrupting its interaction with coactivator CBP/p300. *Mol Cell Biol.* 2014;34(6):1085-99.
64. Pawlus MR, Wang L, and Hu CJ. STAT3 and HIF1alpha cooperatively activate HIF1 target genes in MDA-MB-231 and RCC4 cells. *Oncogene.* 2014;33(13):1670-9.
65. Rasbach KA, Gupta RK, Ruas JL, Wu J, Naseri E, Estall JL, et al. PGC-1alpha regulates a HIF2alpha-dependent switch in skeletal muscle fiber types. *Proc Natl Acad Sci U S A.* 2010;107(50):21866-71.
66. Call JA, Eckhoff MD, Baltgalvis KA, Warren GL, and Lowe DA. Adaptive strength gains in dystrophic muscle exposed to repeated bouts of eccentric contraction. *J Appl Physiol (1985).* 2011;111(6):1768-77.
67. Pasut A, Jones AE, and Rudnicki MA. Isolation and culture of individual myofibers and their satellite cells from adult skeletal muscle. *J Vis Exp.* 2013(73):e50074.
68. Motohashi N, Asakura Y, and Asakura A. Isolation, culture, and transplantation of muscle satellite cells. *J Vis Exp.* 2014(86).
69. Gage GJ, Kipke DR, and Shain W. Whole animal perfusion fixation for rodents. *J Vis Exp.* 2012(65).

## FIGURES AND FIGURE LEGENDS

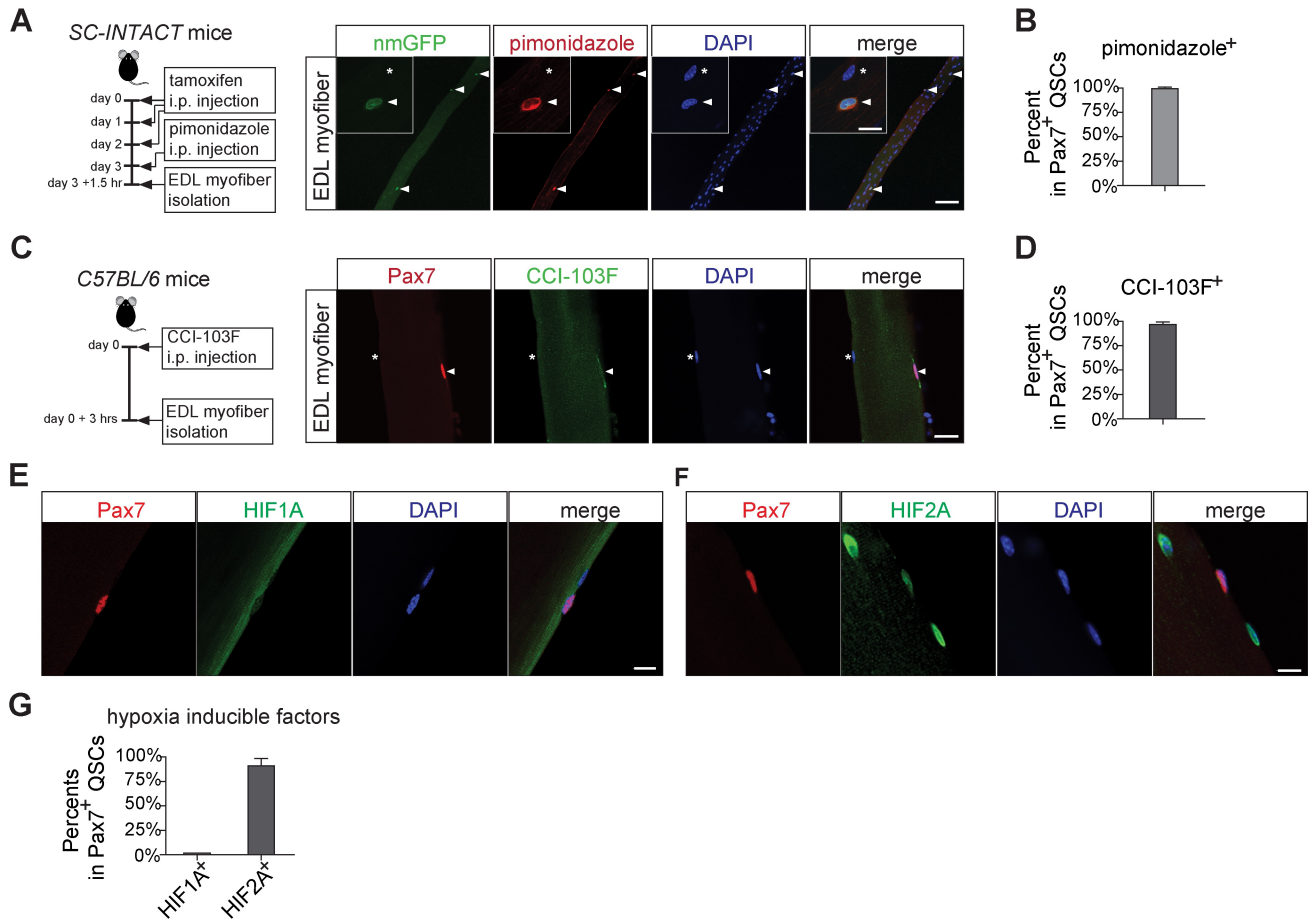


**Figure 1. Quiescent satellite cells are hypoxic in the niche and express HIF2A, but not HIF1A**

(A) A timeline of in vivo pimonidazole labeling in *SC-INTACT* mice and representative confocal images of uninjured/resting EDL myofibers ( $n > 50$  myofibers from  $n = 3$  mice) showing nmGFP<sup>pos</sup> QSCs are pimonidazole<sup>pos</sup>. Scale bar: 50  $\mu$ m. Insets: pimonidazole signals are relatively enriched in the cytoplasm of a QSC. Arrowheads: QSCs; asterisk: myonucleus. Scale bar: 10  $\mu$ m.

(B) The percent of pimonidazole<sup>pos</sup> QSCs.

(C) A timeline of in vivo CCI-103F labeling in *C57BL/6* mice and representative images of uninjured/resting EDL myofibers ( $n > 50$  myofibers from  $n = 3$  mice) showing nmGFP<sup>pos</sup> QSCs are CCI-103F<sup>pos</sup>. Arrowhead: QSC; asterisk: myonucleus. Scale bar: 20  $\mu$ m.

(D) The percent of CCI-103F<sup>pos</sup> QSCs.

(E-F) Representative images of uninjured/resting EDL myofibers from *C57BL/6* mice (n>50 myofibers from n=6 mice/group) showing most QSCs are HIF2A<sup>+pos</sup> but HIF1A<sup>-neg</sup>. Scale bars: 10  $\mu$ m.

(G) Percents of HIF1A<sup>+pos</sup> and HIF2A<sup>+pos</sup> QSCs.

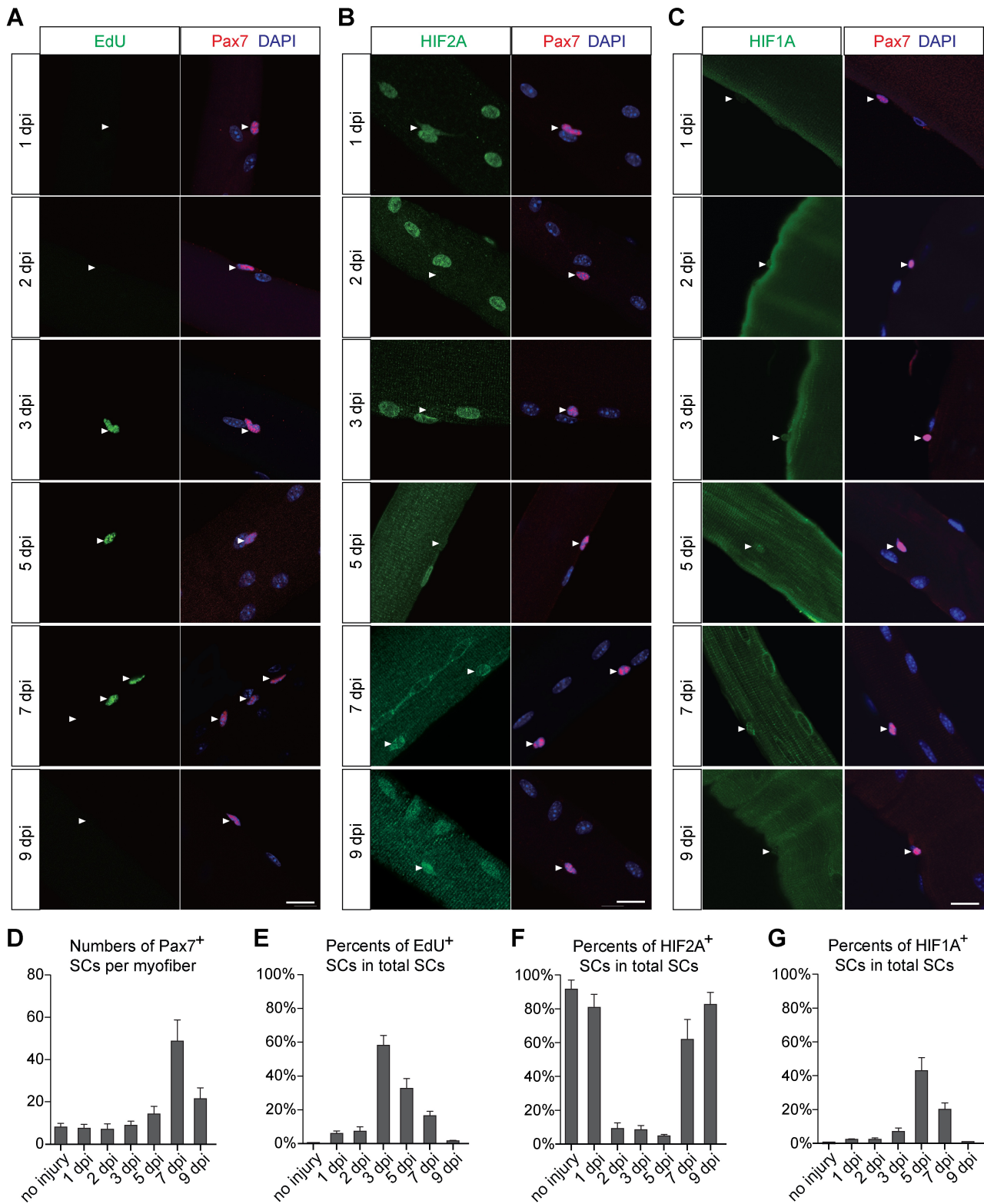


**Figure 2. Muscle repair following eccentric contraction-induced injury is concomitant with dynamic alterations of HIF2A and HIF1A expression in satellite cells**

(A-C) Representative images of EDL myofibers from injured muscles at various time points (n>50 myofibers from n=3 mice/group/time point) and stained for Pax7, DAPI and EdU (B) or HIF2A (C) or HIF1A (D). Arrowheads: SCs. Scale bars: 20  $\mu$ m.

(D) Numbers of Pax7<sup>+pos</sup> SCs per myofiber at various time points.

(E) Percents of EdU<sup>+pos</sup> SCs at various time points.

(F) Percents of HIF2A<sup>+pos</sup> SCs at various time points.

(G) Percents of HIF1A<sup>+pos</sup> SCs at various time points.

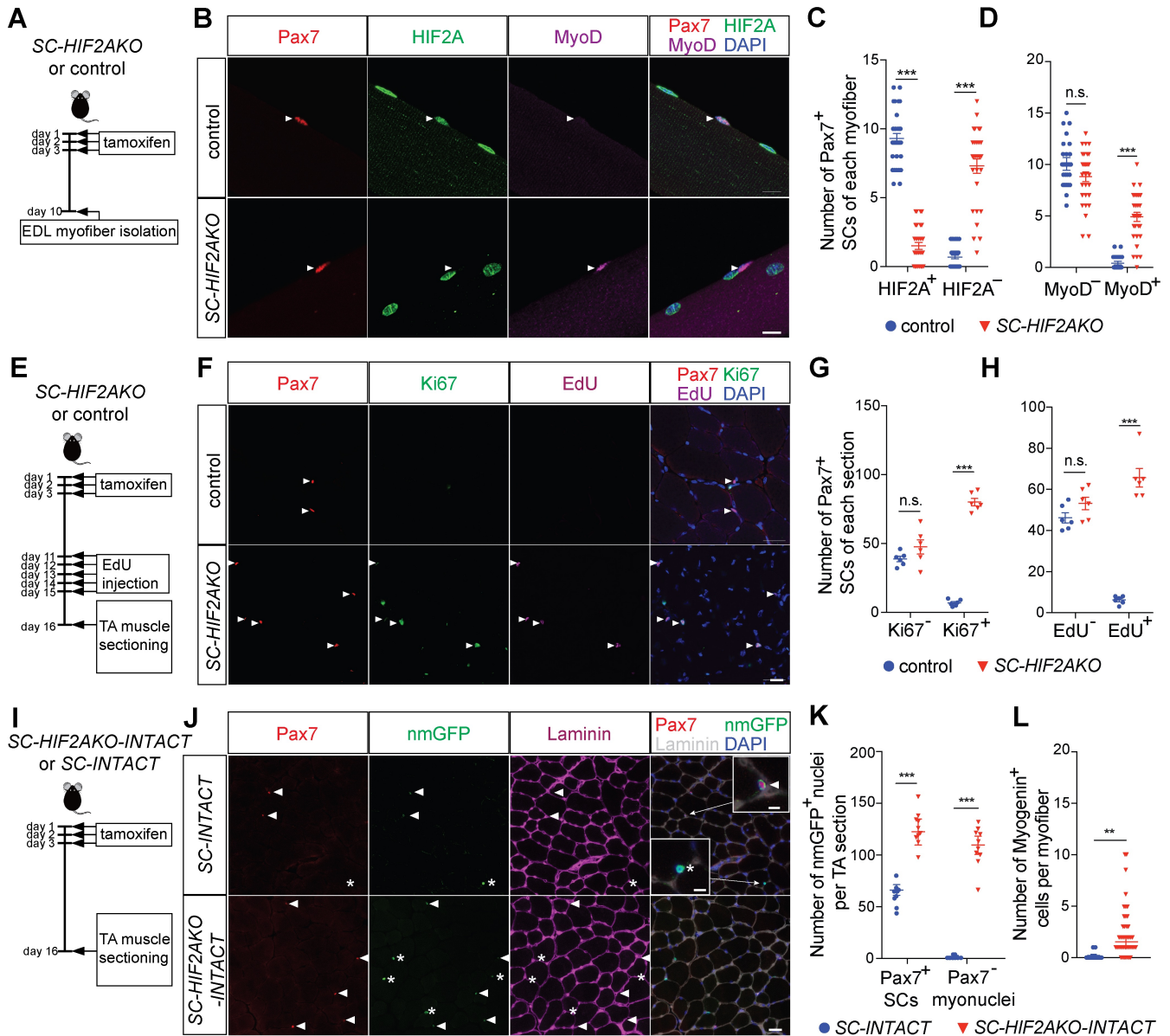


**Figure 3. Genetic ablation of HIF2A in QSCs leads to transient activation, proliferation and differentiation of SCs**

(A) A timeline of genetic ablation of HIF2A in QSCs.

(B) Representative images of myofibers from *SC-HIF2AKO* mice and control littermates ( $n > 50$  myofibers from  $n = 5$  mice/group; 10 dpr). Immunofluorescence of Pax7 (red), HIF2A (green), MyoD (purple) and DAPI (blue) revealed HIF2A<sup>-neg</sup>/MyoD<sup>pos</sup> and HIF2A<sup>pos</sup>/MyoD<sup>-neg</sup> SCs (arrowheads) in *SC-HIF2AKO* and control mice, respectively. Scale bar: 10  $\mu$ m.

(C) Numbers of HIF2A<sup>pos</sup> and HIF2A<sup>-neg</sup> SCs per myofiber (10 dpr).

(D) Numbers of MyoD<sup>-neg</sup> and MyoD<sup>pos</sup> SCs per myofiber (10 dpr).

- (E) A timeline of characterizing SC proliferation after HIF2A-ablation in QSCs.
- (F) Representative cross-sectional images of TA muscles from *SC-HIF2AKO* mice and control littermates (n=6 mice/group; 16 dpr). Immunofluorescence of Pax7 (red), Ki67 (green), EdU (purple) and DAPI (blue) revealed an increase of Ki67<sup>pos</sup>/EdU<sup>pos</sup> SCs (arrowheads) in *SC-HIF2AKO* mice. Scale bar: 20  $\mu$ m.
- (G) Numbers of Ki67<sup>neg</sup> and Ki67<sup>pos</sup> SCs per TA section.
- (H) Numbers of EdU<sup>neg</sup> and EdU<sup>pos</sup> SCs per TA section.
- (I) A timeline of tracing SC fates after HIF2A-ablation in QSCs.
- (J) Representative images of TA muscles from *SC-HIF2AKO-INTACT* and control *SC-INTACT* mice (n=6 mice/group; 16 dpr). Immunofluorescence of nmGFP, Pax7, Laminin B2 and DAPI revealed increased nmGFP<sup>pos</sup>/Pax7<sup>pos</sup> SCs (arrowheads) and nmGFP<sup>pos</sup>/Pax7<sup>neg</sup> myonuclei (asterisks) in *SC-HIF2AKO-INTACT* mice. Scale bar: 20  $\mu$ m. Insets: both nmGFP<sup>pos</sup>/Pax7<sup>pos</sup> SCs and nmGFP<sup>pos</sup>/Pax7<sup>neg</sup> myonuclei are adjacent to the basal lamina. Scale bars: 5  $\mu$ m.
- (K) Numbers of nmGFP<sup>pos</sup>/Pax7<sup>pos</sup> SCs and nmGFP<sup>pos</sup>/Pax7<sup>neg</sup> myonuclei per TA section.
- (L) Numbers of nmGFP<sup>pos</sup>/Myogenin<sup>pos</sup> differentiating SCs per EDL myofiber (16 dpr).
- Statistics in the figure: Student's t-test (two-sided). Error bars: s.e.m.

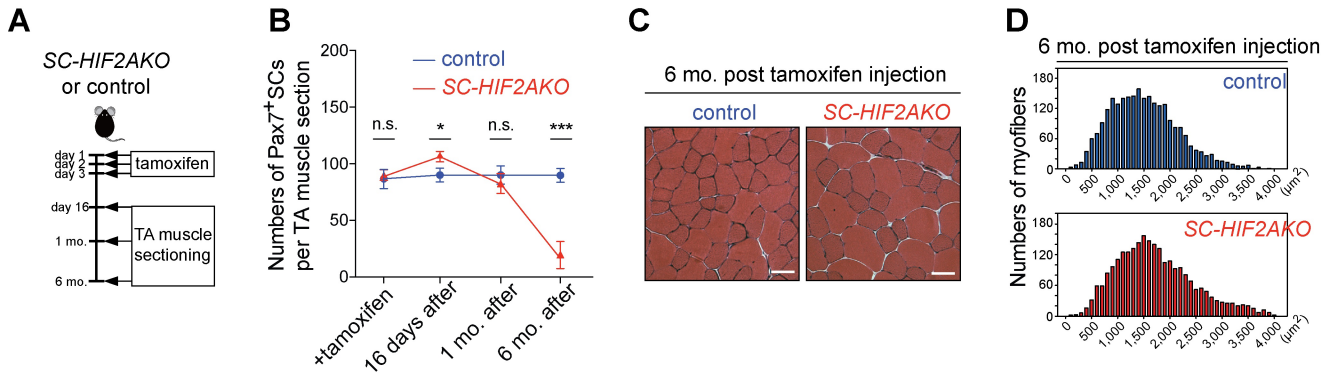


**Figure 4. Long-term ablation of HIF2A results in the loss of SC homeostatic self-renewal**

(A) A timeline of characterizing SC homeostasis after HIF2A ablation in QSCs.

(B) Numbers of Pax7<sup>+</sup> SCs per TA section in SC-HIF2AKO mice and control littermates on the same day of tamoxifen induction (+tamoxifen), at 16 days, 1 month and 6 months after tamoxifen-induced HIF2A ablation (n = 3 mice/group/time point).

(C) H/E staining of TA muscles from SC-HIF2AKO mice and control littermates (n=3 mice/group; at 6 months after tamoxifen-induced HIF2A ablation). Scar bars: 20  $\mu$ m.

(D) Distributions of myofiber cross-sectional areas of TA muscles from SC-HIF2AKO mice and control littermates (n=3 mice/group; at 6 months after tamoxifen-induced HIF2A ablation).

Statistics in the figure: Student's t-test (two-sided). Error bars: s.e.m.

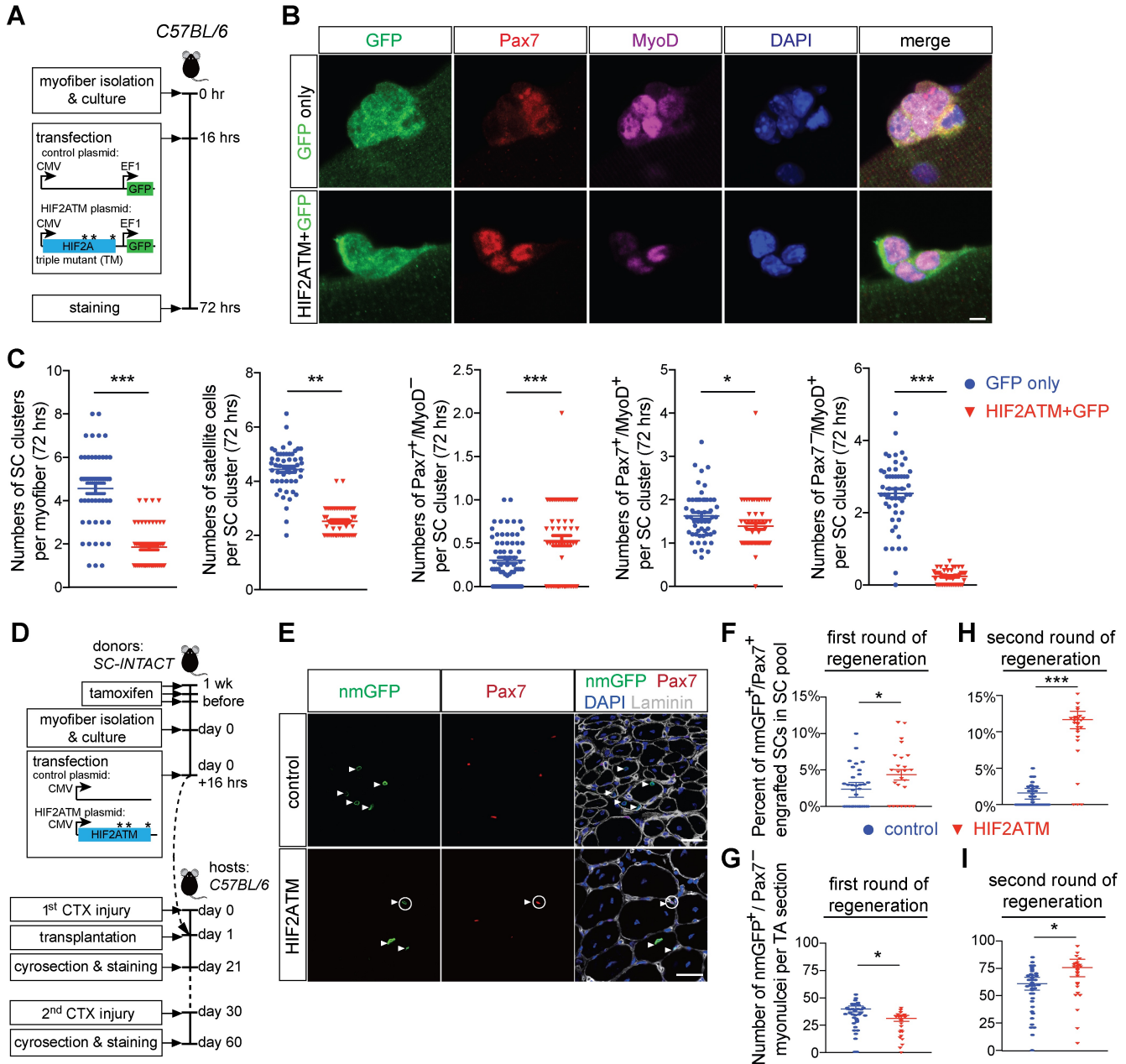


**Figure 5. HIF2A stabilization under normoxia promotes quiescence, self-renewal and stemness of SCs yet impedes myogenic differentiation**

(A) A diagram depicting the timeline and plasmids used for HIF2A stabilization in normoxic SC culture.

(B) Representative images of transfected ( $GFP^{+pos}$ ) SC clusters on myofibers that were from *C57BL/6* mice ( $n > 50$  myofibers from  $n = 7$  mice/group), transfected with either HIF2ATM or control plasmids and stained for Pax7, MyoD and DAPI. Scale bar: 5  $\mu m$ .

(C) From left to right, numbers of SC clusters, Pax7<sup>pos</sup> SCs per cluster, Pax7<sup>pos</sup>/MyoD<sup>neg</sup>, Pax7<sup>pos</sup>/MyoD<sup>pos</sup> and Pax7<sup>neg</sup>/MyoD<sup>pos</sup> SCs per SC cluster (n>50 myofibers).

(D) A diagram showing the experimental scheme for transplanting HIF2A-stabilized SCs and tracing their cell fates in vivo.

(E) Cross-sectional images of TA muscles that were transplanted with HIF2ATM or control plasmid-transfected SCs (n=5 mice/group; 21 days post the 1<sup>st</sup> injury). Immunofluorescence of Pax7 and nmGFP revealed two fates of transplanted SCs: engrafted SCs that retained stemness (nmGFP<sup>pos</sup>/Pax7<sup>pos</sup>; circle; shown in HIF2ATM panels) and engrafted SCs that differentiated into myonuclei (nmGFP<sup>pos</sup>/Pax7<sup>neg</sup>; arrowheads). Note: control and HIF2ATM images have different magnifications. Scale bars: 20  $\mu$ m.

(F, H) Percents of engrafted and self-renewed nmGFP<sup>pos</sup>/Pax7<sup>pos</sup> SCs in total SC pool after the 1<sup>st</sup> round (21 dpi; n=5 mice/group; F) and the 2<sup>nd</sup> round of regeneration (30 dpi; n=6 mice/group; H).

(G, I) Numbers of nmGFP<sup>pos</sup>/Pax7<sup>neg</sup> differentiated myonuclei per TA muscle section after the 1<sup>st</sup> round (G) and the 2<sup>nd</sup> round of regeneration (I).

Statistics in the figure: Student's t-test (two-sided). Error bars: s.e.m.

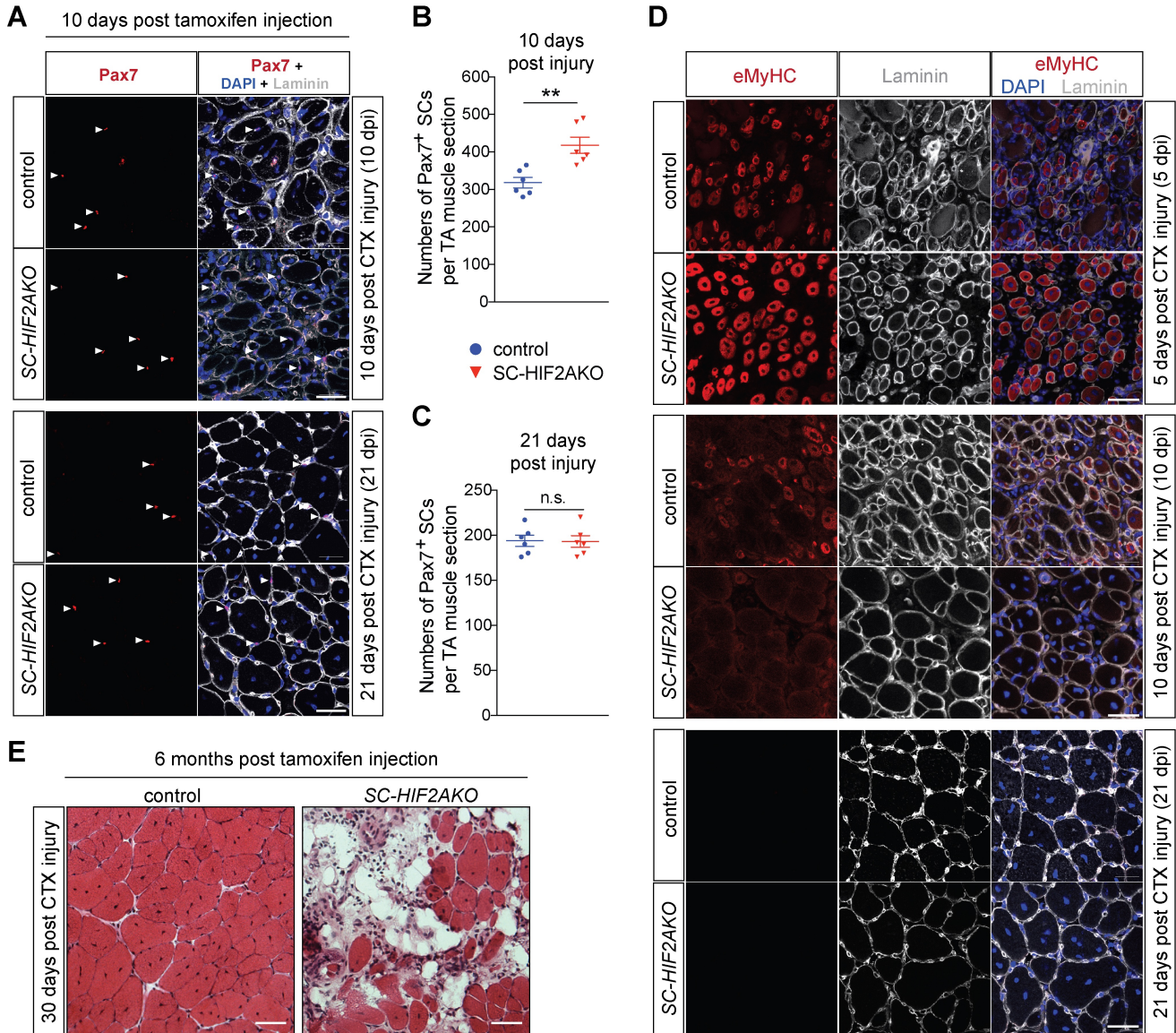


**Figure 6. Genetic ablation of HIF2A transiently improves muscle regeneration but impairs long-term muscle regeneration potential**

(A) Representative images of TA muscles from *SC-HIF2AKO* mice and control littermates (n=6 mice/group/time point) that were injured by CTX at 10 days after tamoxifen-induced HIF2A ablation (10 dpr). Immunofluorescence of Pax7 at 10 days (10 dpi) and 21 days (21 dpi) after CTX injury revealed an increase of Pax7<sup>+</sup> SCs (arrowheads) in *SC-HIF2AKO* mice. Scale bars: 20  $\mu$ m.

(B-C) Numbers of Pax7<sup>+</sup> SCs per TA muscle section at 10 dpi (B) and 21 dpi (C).

(D) Representative images of TA muscles from *SC-HIF2AKO* mice and control littermates (n=6 mice/group/time point) that were injured by CTX at 10 days after tamoxifen-induced HIF2A

ablation (10 dpr). Immunofluorescence of eMyHC and Laminin B2 at 5 days (5 dpi), 10 days (10 dpi) and 21 days (21 dpi) after CTX injury revealed accelerated muscle regeneration in *SC-HIF2AKO* mice. Scale bars: 20  $\mu$ m.

(E) Representative images of TA muscles *SC-HIF2AKO* mice and control littermates (n=3 mice/group) that were injured by CTX at 6 months after tamoxifen-induced HIF2A ablation. H/E staining of TA muscles at 30 days after CTX injury (30 dpi) revealed impaired muscle regeneration in *SC-HIF2AKO* mice. Scale bars: 20  $\mu$ m.

Statistics in the figure: Student's t-test (two-sided). Error bars: s.e.m.

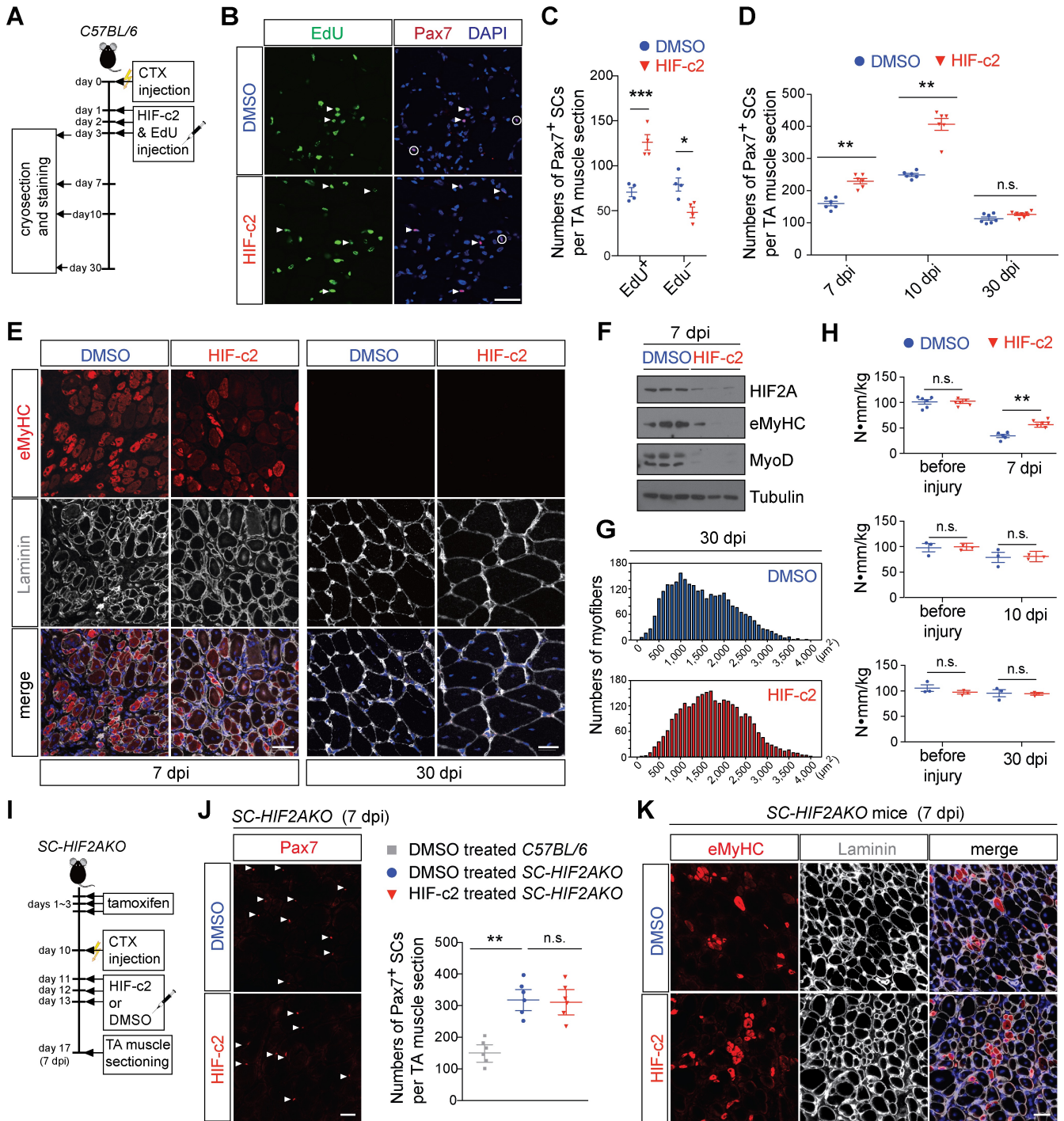


**Figure 7. Transient pharmacological inhibition of HIF2A in CTX-injured muscle promotes SC proliferation and accelerates muscle regeneration**

(A) A timeline of pharmacological inhibition of HIF2A after CTX-induced muscle injury in *C57BL/6* mice.

- (B) Representative images of HIF-c2 or 1% DMSO-treated TA muscles (3 dpi) from *C57BL/6* mice (n=6 mice/group). Immunofluorescence revealed increased Pax7<sup>pos</sup>/EdU<sup>pos</sup> proliferative SCs (arrowheads) and decreased Pax7<sup>pos</sup>/EdU<sup>neg</sup> QSCs (circles). Scale bar: 20  $\mu$ m.
- (C) Numbers of EdU<sup>pos</sup> and EdU<sup>neg</sup> SCs per TA muscle section at 3 dpi (n=6).
- (D) Numbers of Pax7<sup>pos</sup> SCs per TA muscle section at 7 dpi, 10 dpi and 30 dpi (n=6 or 7).
- (E) Representative eMyHC and Laminin B2 immunofluorescence in HIF-c2 or DMSO-treated TA muscles at 7 dpi and 30 dpi (n=3). Scale bars: 20  $\mu$ m.
- (F) Immunoblotting showing the expression levels of HIF2A, eMyHC, MyoD and Tubulin in HIF-c2 or DMSO-treated TA muscles at 7 dpi (n=3).
- (G) Distributions of myofiber cross-sectional areas of HIF-c2 or DMSO-treated TA muscles at 30 dpi (n=3).
- (H) The maximal torques of uninjured TA muscles and HIF-c2 or DMSO-treated TA muscles at 7 dpi (n=6), 10 dpi (n=3) and 30 dpi (n=3).
- (I) A timeline of pharmacological inhibition of HIF2A after CTX-induced muscle injury in *C57BL/6* mice and *SC-HIF2AKO* mice.
- (J) Left: representative Pax7 immunofluorescence in HIF-c2 or DMSO-treated TA muscles from *SC-HIF2AKO* mice (n=6 mice/group) at 10 dpi; right: numbers of Pax7<sup>pos</sup> SCs per TA muscle section at 7 dpi. Scale bar: 20  $\mu$ m.
- (K) Representative eMyHC and Laminin B2 immunofluorescence in HIF-c2 or DMSO-treated TA muscles from *SC-HIF2AKO* (n=6 mice/group) at 7 dpi.
- Statistics in the figure: Student's t-test (two-sided). Scale bar: 20  $\mu$ m. Error bars: s.e.m.

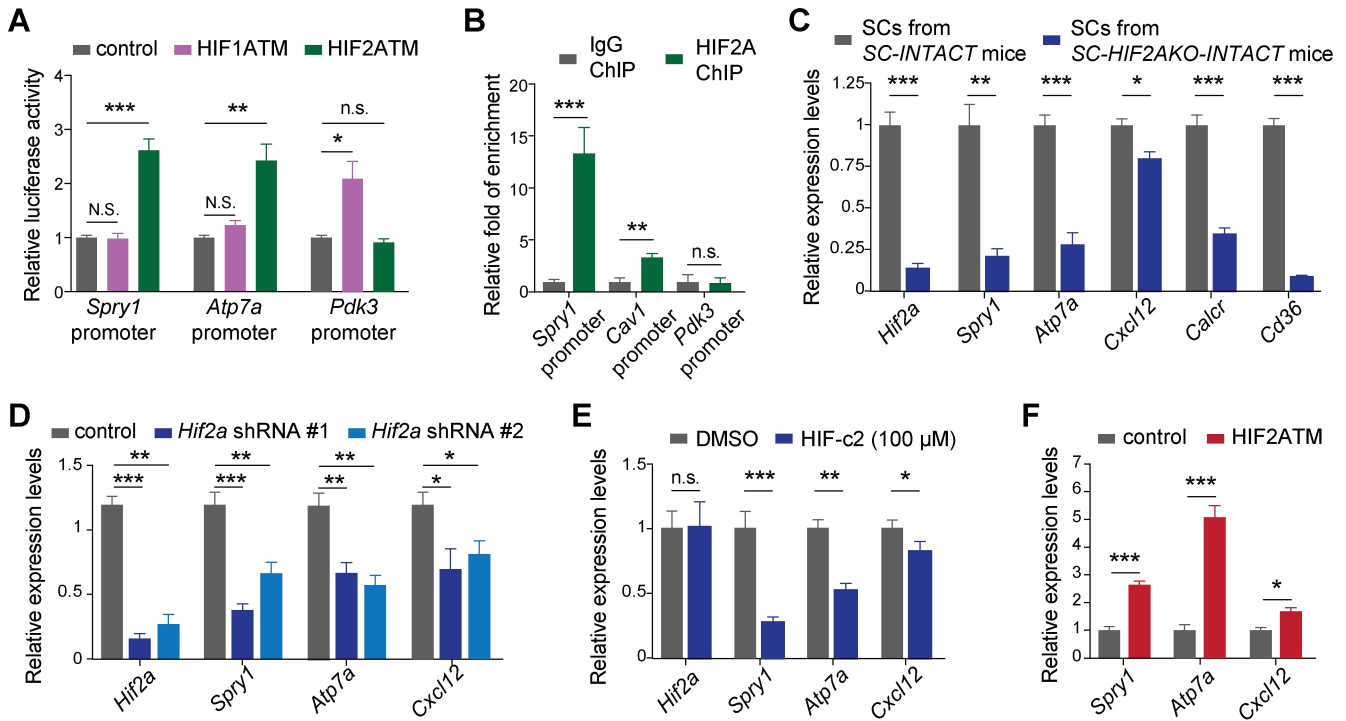


**Figure 8. *Spry1* is a novel target of HIF2A in QSCs**

(A) Luciferase assays show that stabilized expression HIF2A (HIF2ATM), but not HIF1A (HIF1ATM), increased the promoter activities of *Spry1* and *Atp7a* (a known HIF2A target). In contrast, HIF1A, but not HIF2A, transactivates *Pdk3* promoter.

(B) ChIP-qPCR indicate that HIF2A binds the promoters of *Spry1* and *Cav1* (a known HIF2A target), but not the *Pdk3* promoter, in quiescent SCs in vivo.

(C) RT-qPCR reveal that HIF2A ablation in QSCs in vivo reduced mRNA levels of *HIF2A*, *Spry1*, *Calcr*, and *Cd36*.

(D) RT-qPCR indicate that two HIF2A shRNAs reduced mRNA levels of *HIF2A* and *Spry1* as well as two known HIF2A targets, *Atp7a* and *Cxcl12*, in C2C12 myoblasts.

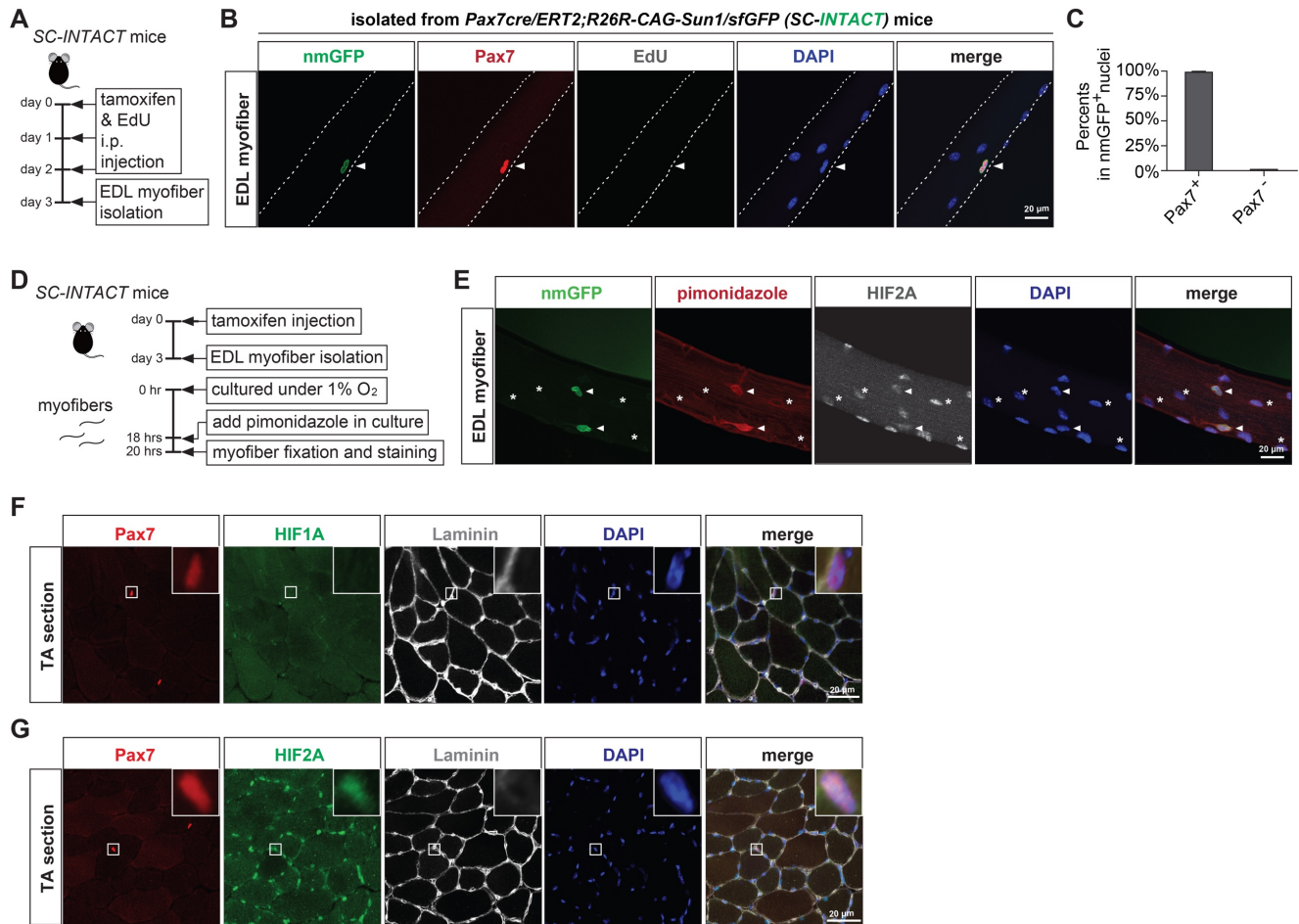
(E) RT-qPCR reveal that HIF-c2 treatment decreased mRNA levels of HIF2A targets, *Spry1*, *Atp7a* and *Cxcl12* in C2C12 myoblasts.

(F) RT-qPCR indicate that HIF2ATM increased mRNA levels of *Spry1* as well as two known HIF2A targets, *Atp7a* and *Cxcl12*, in C2C12 myoblasts.

Statistics in the figure: Student's t-test (two-sided). Error bars: s.e.m.

## SUPPLEMENTARY FIGURES AND LEGENDS

### Supplementary Fig. 1



### Supplementary Figure 1. Genetic tagging and labeling of satellite cell nuclear membrane and pimonidazole labeling of single isolated myofibers cultured under hypoxia.

(A) A diagram showing the genetic tagging and labeling of the nuclear membrane of quiescent SCs.

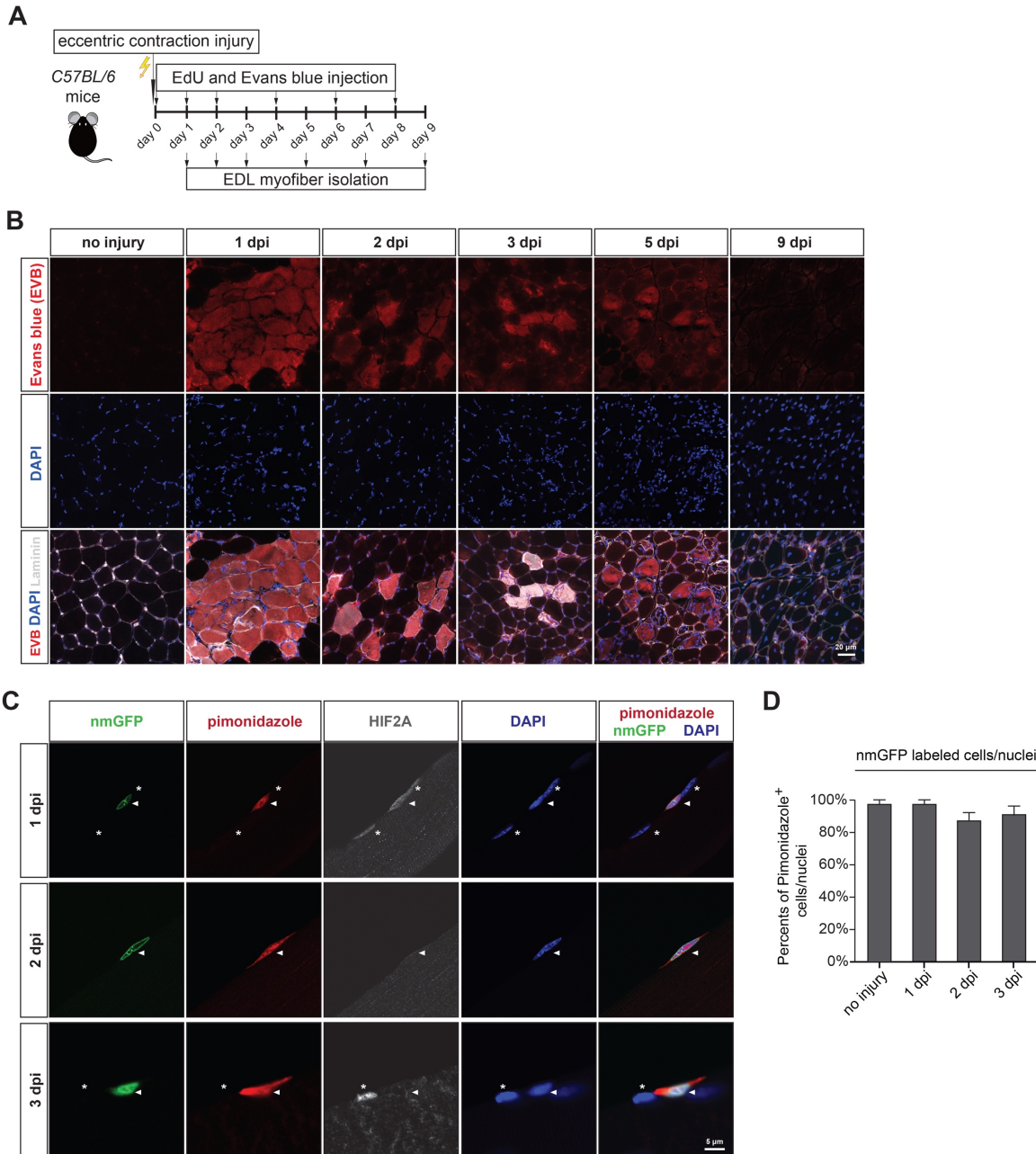
(B) Representative confocal images of uninjured EDL myofibers isolated from tamoxifen injected *Pax7cre/ERT2;R26R-CAG1-Sun1/sfGFP* (SC-INTACT) mice (n>50 myofibers from n=5 mice; after 3 consecutive days of tamoxifen and EdU injection). Immunofluorescence of Pax7, EdU and DAPI indicate that tamoxifen-induced expression of Sun1/sfGFP fusion protein specifically localizes to the nuclear membrane of satellite cells, which is cell cycle independent (labeled SCs are EdU<sup>-neg</sup>). Arrowhead: satellite cell.

(C) Percents of Pax7<sup>+pos</sup> nuclei (SC nuclei) and Pax7<sup>-neg</sup> nuclei (myonuclei) in total nmGFP<sup>+pos</sup> nuclei on uninjured EDL myofibers.

(D) A diagram summarizing the experimental procedure of pimonidazole labeling of single isolated myofibers cultured under hypoxia (1% O<sub>2</sub>) for 20 hrs. Pimonidazole was added to the myofiber culture for the last 1.5 hrs to mimic the condition of in vivo pimonidazole labeling.

(E) Representative confocal images of EDL myofibers that were isolated from tamoxifen injected SC-*INTACT* mice (n>50 myofibers from n=3 mice), cultured under hypoxia, labeled with pimonidazole (50 μM). Fluorescent imaging reveals that nmGFP<sup>+pos</sup> SCs (arrowheads) are hypoxic (pimonidazole<sup>+pos</sup>) whereas myonuclei (asterisks) are pimonidazole<sup>-neg</sup>.

(F-G) Representative cross-sectional images of uninjured TA muscles from *C57BL/6* mice (n=3 mice) with immunofluorescence of Pax7, HIF1A (F) or HIF2A (G), Laminin B2 and DAPI. Insets: zoomed-in images of quiescent SCs.



**Supplementary Figure 2. Satellite cells maintain the hypoxic state when HIF2A expression diminishes upon eccentric contraction-induced injury.**

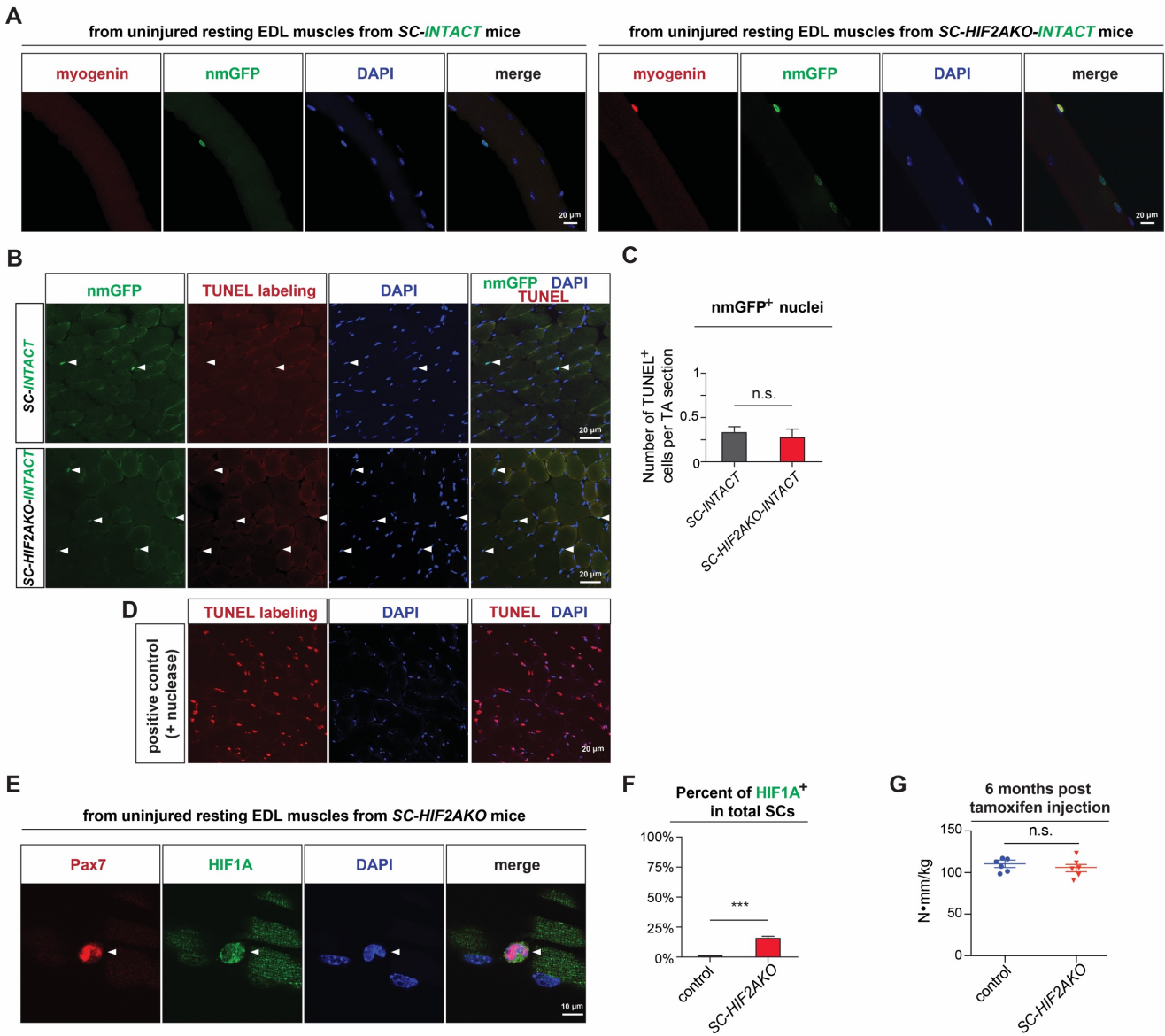
(A) A timeline of characterizing SC dynamics after eccentric contraction-induced muscle injury. For each time point, EdU and Evans blue were injected 24 hrs before myofiber isolation.

(B) Representative cross-sectional images of uninjured and eccentric contraction-injured TA muscles (at 1, 2, 3, 4, 5, 9 dpi) from *C57BL/6* mice (n=3 mice/group) showing the fluorescence of Evans blue, Laminin B2 and DAPI.

(C) Representative images of EDL myofibers isolated from tamoxifen injected *SC-INTACT* mice at 1, 2 and 3 days post eccentric contraction-induced injury ( $n > 50$  myofibers;  $n = 3$  mice/time point). Pimonidazole was i.p. injected 1.5 hrs before euthanasia. nmGFP fluorescence and immunofluorescence of pimonidazole and HIF2A indicate that SCs maintain the pimonidazole<sup>+pos</sup> hypoxic state from 1 dpi to 3 dpi, whereas HIF2A expression diminishes in hypoxic SCs at 2 dpi and 3 dpi. Arrowheads: SCs; asterisks: myonuclei.

(D) Percents of pimonidazole<sup>+pos</sup> cells in nmGFP labeled cells on uninjured EDL myofibers and myofibers at 1-3 dpi.

### Supplementary Fig. 3



### Supplementary Figure 3. SC-specific ablation of HIF2A leads to increased Myogenin and HIF1A expression, but does not results in SC apoptosis.

(A) Representative images of uninjured EDL myofibers isolated from tamoxifen injected *SC-HIF2AKO-INTACT* mice and control *SC-INTACT* mice ( $n > 50$  myofibers from  $n = 3$  mice/group; at 16 dpr). Fluorescence of nmGFP and Myogenin indicate that some nmGFP-labeled SCs are Myogenin<sup>+</sup>pos.

(B) Representative cross-sectional images of uninjured TA muscles from tamoxifen injected *SC-HIF2AKO-INTACT* mice and control *SC-INTACT* mice ( $n = 3$  mice/group; at 16 dpr) showing

nmGFP<sup>pos</sup> cells (SC lineage; arrowheads) lack of the fluorescence of TUNEL labeling.  
Arrowheads: nmGFP<sup>pos</sup> cells.

(C) Percents of TUNEL<sup>pos</sup>/nmGFP<sup>pos</sup> cells in *SC-HIF2AKO-INTACT* mice and control *SC-INTACT* mice.

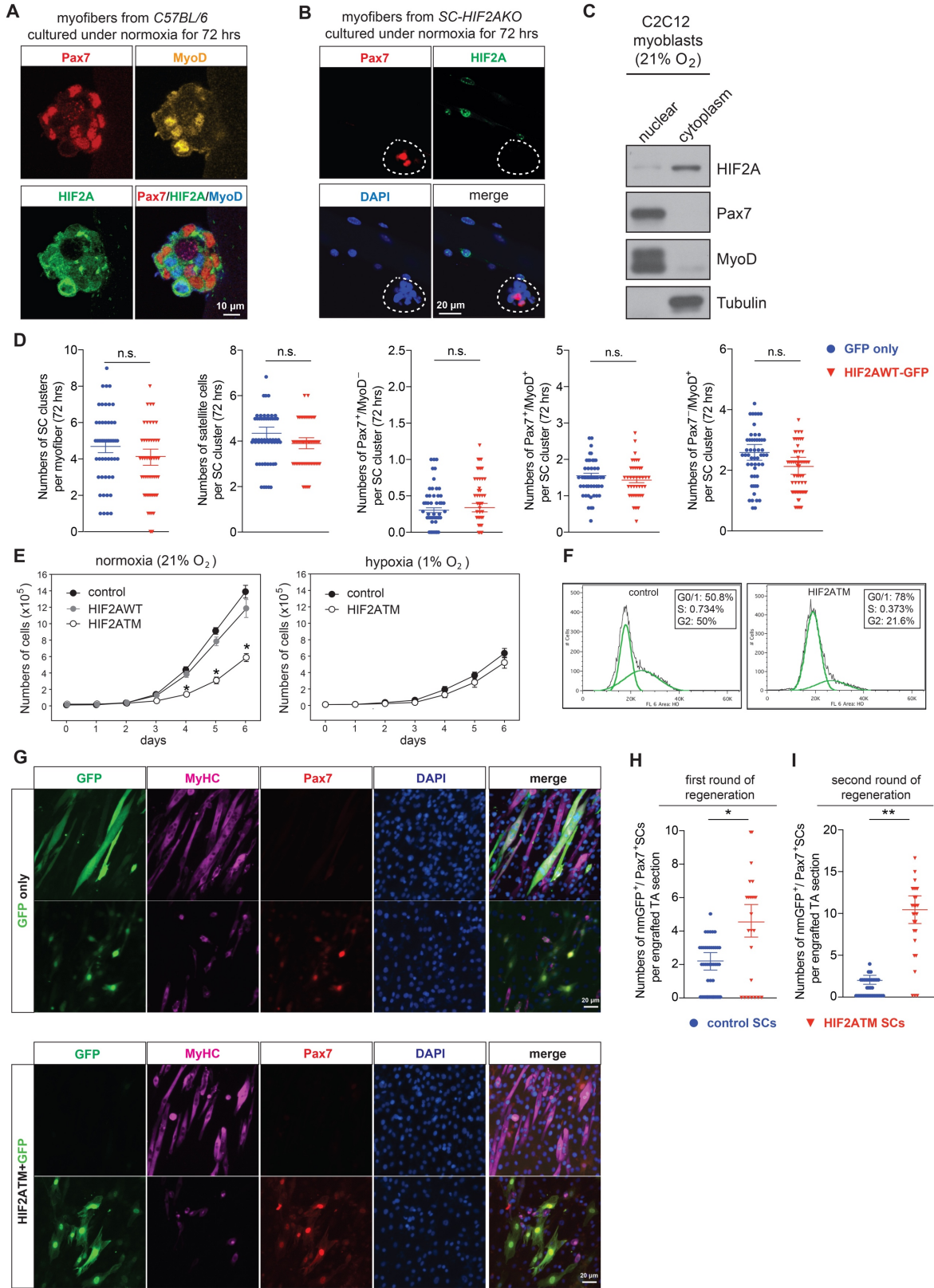
(D) Representative images of the technical positive control for TUNEL labeling showing pronounced fluorescence of TUNEL labeling after nuclease treatment.

(E) Representative images of uninjured EDL myofibers isolated from tamoxifen injected *SC-HIF2AKO* mice (n>50 myofibers from n=3 mice; at 16 dpr). Immunofluorescence of Pax7 and HIF1A indicate that some Pax7<sup>pos</sup> SCs are HIF1A<sup>pos</sup>. Arrowheads: SC.

(F) Percents of HIF1A<sup>pos</sup> SCs in *SC-HIF2AKO* mice and the control littermates.

(G) The maximal torque of uninjured TA muscles from *SC-HIF2AKO* mice and age-matched control littermates (n=6 mice/group) at 6 months after tamoxifen -nduced recombination.

Supplementary Fig. 4



**Supplementary Figure 4. HIF2A localizes in the cytoplasm of cultured SCs and C2C12 myoblasts under normoxia (21% pO<sub>2</sub>) and effects of transfection of wildtype and O<sub>2</sub>-insensitive HIF2A in primary and C2C12 myoblasts.**

(A) Representative images of a SC cluster on myofibers isolated from *C57BL/6* mice (n>50 clusters from n=3 mice) and cultured for 72-hrs under normoxia showing immunofluorescence of Pax7, MyoD, HIF2A and DAPI. Notably, HIF2A immunofluorescence localizes mostly in the cytoplasm, which is distinct from the nuclear localization of Pax7 and MyoD.

(B) Representative images of a SC cluster on myofibers isolated from tamoxifen injected SC-*HIF2AKO* mice (n>50 clusters from n=3 mice; at 10 dpr) and cultured for 72-hrs under normoxia showing immunofluorescence of Pax7, HIF2A and DAPI.

(C) Immunoblotting of Pax7, MyoD, HIF2A and Tubulin in nuclear and cytoplasmic fractions of C2C12 myoblasts cultured under normoxia.

(D) From left to right, numbers of SC clusters, Pax7<sup>pos</sup> SCs per cluster, Pax7<sup>pos</sup>/MyoD<sup>neg</sup>, Pax7<sup>pos</sup>/MyoD<sup>pos</sup> and Pax7<sup>neg</sup>/MyoD<sup>pos</sup> SCs per SC cluster (n>50 myofibers) after transfection of wildtype HIF2A in SCs cultured for 72-hrs under normoxia.

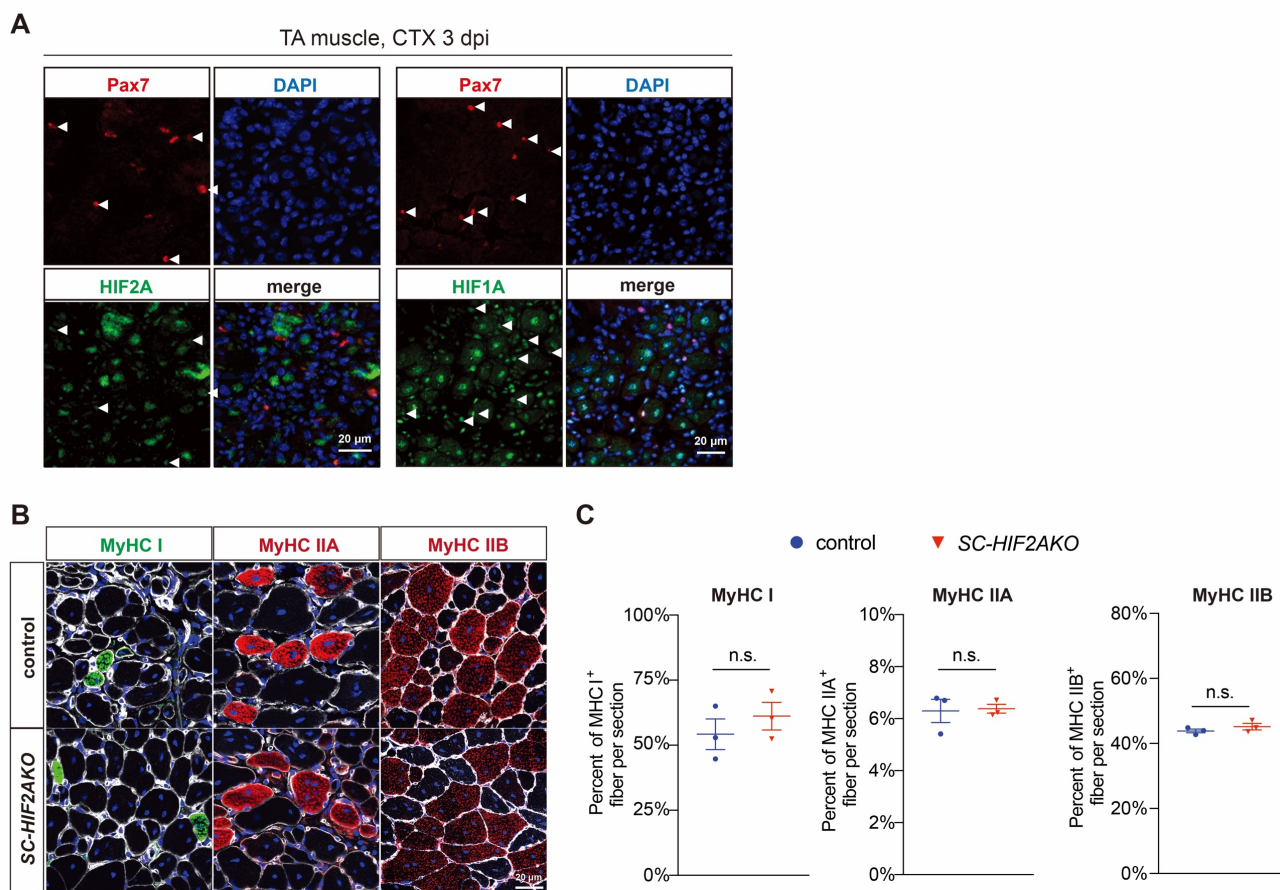
(E) Numbers of primary myoblasts after transfection of control, wildtype HIF2A (HIF2AWT) and O<sub>2</sub>-insensitive HIF2A (HIF2ATM) and cultured under normoxia or hypoxia (1% O<sub>2</sub>) for 1-6 days (1x10<sup>4</sup> seeded at day 0; n=6 replicates).

(F) Histograms of Hoeschst 33258 intensity distribution in control and HIF2ATM transfected primary myoblasts and results of cell cycle analysis (FlowJo).

(G) Representative images of C2C12 myoblasts transfected with control or HIF2ATM plasmids and differentiated in 2% horse serum for 5 days. Non-transfected (GFP<sup>neg</sup>) and transfected (GFP<sup>pos</sup>) cells were immunostained for MyHC, Pax7 and DAPI.

(H, I) Numbers of nmGFP<sup>pos</sup>/Pax7<sup>pos</sup> engrafted SCs per TA muscle section after the 1<sup>st</sup> round (at 21 dpi; n=5 mice/group; H) and the 2<sup>nd</sup> round of regeneration (at 30 dpi; n=6 mice/group; I).

## Supplementary Fig. 5



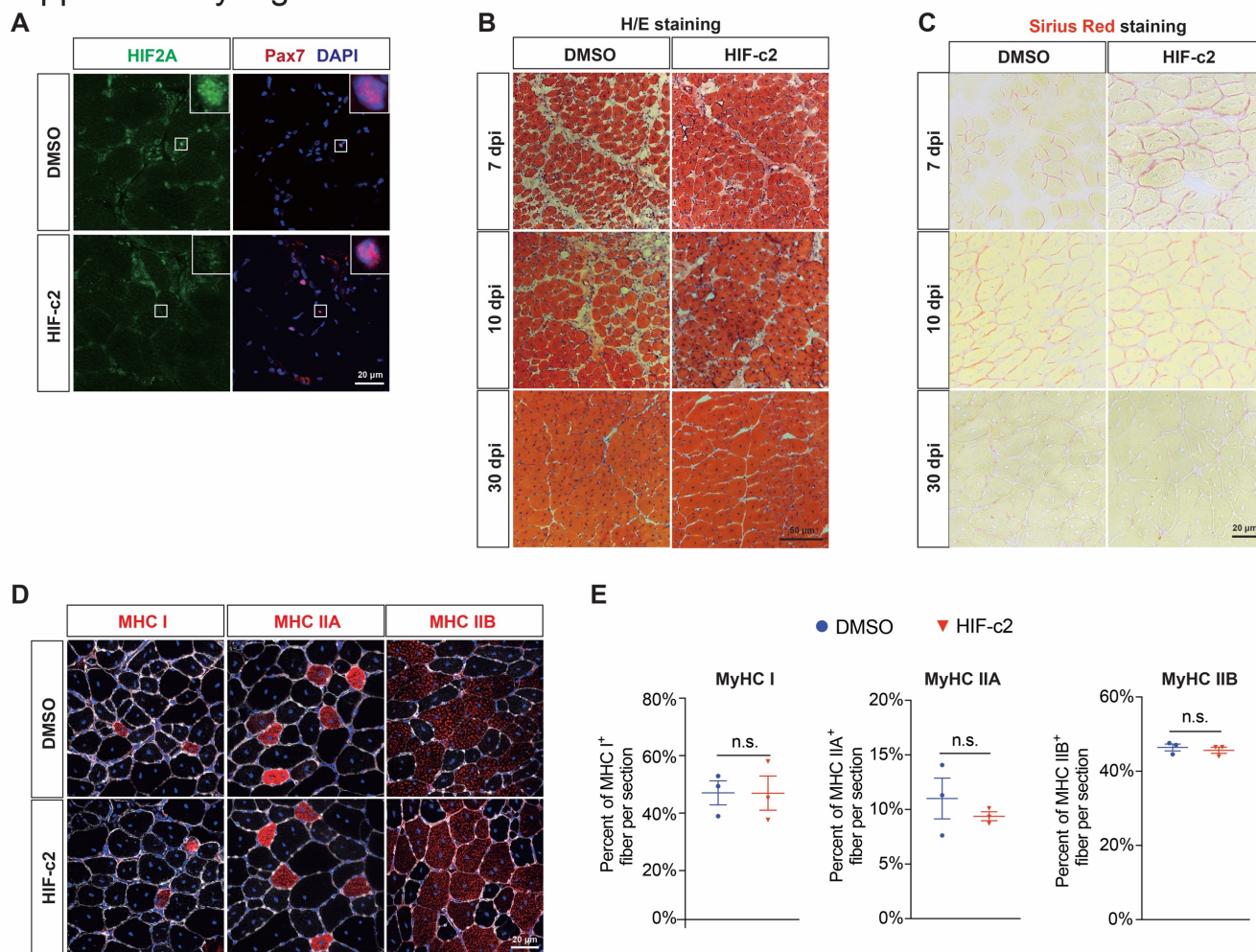
**Supplementary Figure 5. HIF expression in activated satellite cells after CTX-induced injury and compositions of MyHC I, IIA and IIB-positive myofibers after muscle regeneration of *SC-HIF2AKO* mice.**

(A) Representative cross-sectional images of CTX-injured TA muscles (at 3 dpi) from *C57BL/6* mice (n=6 mice/group) showing immunofluorescence of Pax7, HIF2A or HIF1A and DAPI. Arrowheads: SCs.

(B) Representative cross-sectional images of TA muscles (at 30 dpi) from *SC-HIF2AKO* mice and control littermates (n=3 mice/group) showing immunofluorescence of type I MyHC, type IIA MyHC or type IIB MyHC along with Laminin B2 and DAPI.

(C) The percents of myofibers positive for type I MyHC, type IIA MyHC or type IIB MyHC.

## Supplementary Fig. 6



**Supplementary Figure 6. Inhibition of HIF2A by HIF-c2, muscle morphology, collagen content and myofiber type composition of HIF-c2-treated muscle during or after regeneration.**

(A) Representative cross-sectional images of 1% DMSO treated or HIF-c2 treated uninjured TA muscles from *C57BL/6* mice (n=3 mice/group) showing immunofluorescence of Pax7, HIF2A and DAPI. Insets are zoomed-in images of SCs.

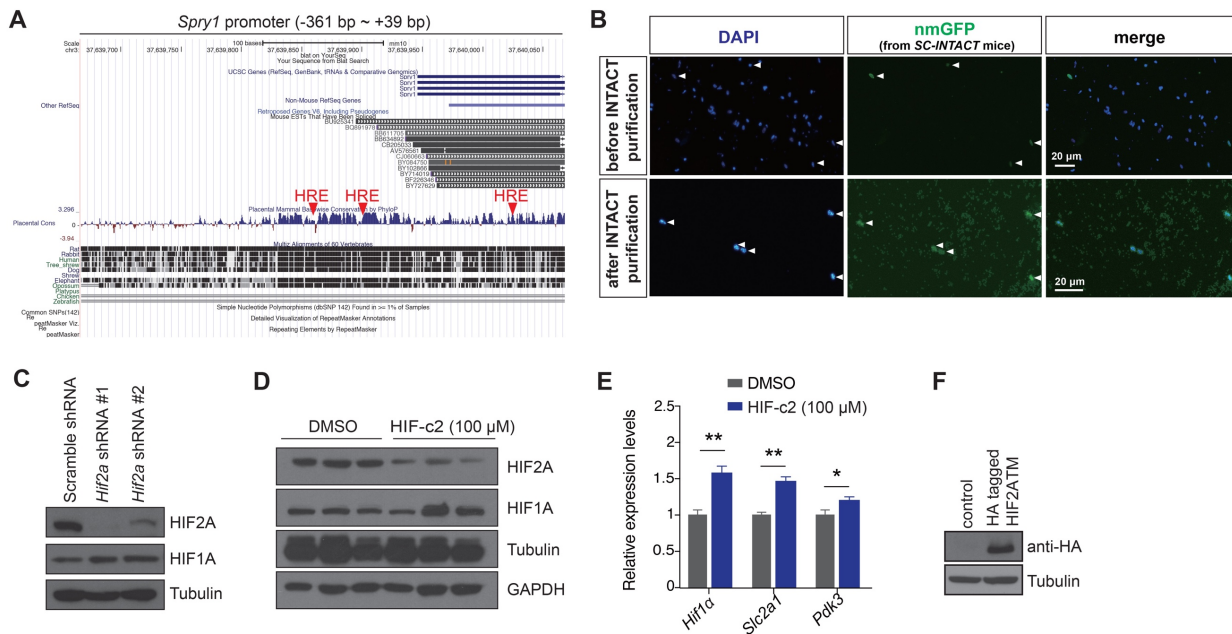
(B) Representative images of H/E staining of CTX-injured TA muscle cross-sections (at 7, 10 and 30 dpi) from *C57BL/6* mice (n=3 mice/group) that were treated by 1% DMSO or HIF-c2.

(C) Representative images of Sirius Red staining (for collagen) of CTX-injured TA muscle cross-sections (at 7, 10 and 30 dpi) from *C57BL/6* mice (n=3 mice/group) that were treated by 1% DMSO or HIF-c2.

(D) Representative cross-sectional images of CTX-injured TA muscles (at 30 dpi) that were treated with 1% DMSO or HIF-c2, showing immunofluorescence of type I MyHC, type IIA MyHC or type IIB MyHC along with Laminin B2 and DAPI.

(E) The percents of myofibers positive for type I MyHC, type IIA MyHC or type IIB MyHC.

## Supplementary Fig. 7



**Supplementary Figure 7. HIF2A binds to HREs in *Spry1* promoter, isolation of nuclei tagged in specific cell types (INTACT) for SCs and reduced HIF2A expression in HIF2A shRNA expressing or HIF-c2 treated C2C12 myoblasts.**

(A) A view from UCSC genome browser showing positions of three Hypoxia-Response Elements (HREs; red) in the *Spry1* proximal promoter (mouse genome).

(B) Representative images showing ratios of nmGFP<sup>pos</sup> SC nuclei and nmGFP<sup>neg</sup> nuclei (including myonuclei and nuclei from other types of cells in muscle) from *SC-INTACT* mice before and after INTACT purification with magnetic Dynabeads. Notably, nmGFP<sup>pos</sup> SC nuclei were affinity attached to Dynabeads (dots with weak green autofluorescence) by anti-GFP/anti-Myc antibodies and were enriched after purification.

(C) Immunoblotting of HIF2A, HIF1A and Tubulin in C2C12 myoblasts transduced with retrovirus expressing control or HIF2A shRNAs (#1 and #2).

(D) Immunoblotting of HIF2A, HIF1A, Tubulin and GAPDH in C2C12 myoblasts, which were treated with HIF-c2 or 1% DMSO (n=3 independent treatments/group).

(E) RT-qPCR assays reveal increased mRNA levels of *HIF1A* and *HIF1A* target genes, *Slc2a1/Glut1* and *Pdk3* in C2C12 myoblasts in response to HIF-c2 (100 μM) treatment.

(F) Immunoblotting (using an antibody against HA-tag) showing HA-tagged HIF2ATM is ectopically expressed in C2C12 myoblasts.

